APPENDIX H8

Salt balance of Northern Spencer Gulf

APPENDIX H8.1

Long-term effects of desalination and climate change

The Effects of Desalination and Climate Change on the Long-Term Salt Balance of Northern Spencer Gulf

RICHARD. A. NUNES-VAZ

EXECUTIVE SUMMARY

This report examines the potential impacts of desalination and climate change on the large-scale, long-term salt balance of northern Spencer Gulf (NSG), addressing the following three issues:

- how rapidly Spencer Gulf responds to influences that disturb its salinity, and how long it takes to 'recover' following a disturbance
- the degree or extent to which salinity is expected to change in response to a disturbance, and
- whether anticipated perturbations associated with desalination and climate change will be large enough to shift the Gulf's salinity, irreversibly, to a new equilibrium state.

Spencer Gulf experiences higher salinities than the adjacent ocean due to a net loss of freshwater from evaporation. This fluid loss is replaced by an influx of seawater at a mean velocity ~$10^{-3}ms^{-1}$ (Nunes & Lennon, 1986) which brings additional salt that must be ejected by oceanographic mechanisms.

The annual and inter-annual variations of salinity of the whole body of NSG were determined by spatial interpolation of field data collected on twelve occasions during the 1980s (Nunes, 1985) and from two new surveys in 2008 and 2009. All salinity data were collected and cross-referenced by the same investigator, using the same calibration instruments and standards, thereby producing an internally-consistent dataset spanning 27 years.

Assuming that the mean salinity of NSG is governed by the cumulative effects of net evaporation, a correlation between NSG salinity in the 1980s, and net evaporation measured by the Bureau of Meteorology at Price (~250km from NSG) was determined. The correlation was greatest (with a coefficient of 0.89) when daily net evaporation was averaged over the six months (192 days) prior to any salinity observation. Continuing the averaging of Price net evaporation through to 2009, it was shown that the more recent observations of NSG salinity remain consistent with the 1980s relationship.

Thus, despite large inter-annual and decadal trends in the records, it is apparent that NSG mean salinity on any particular day is primarily determined by the cumulative effects of net evaporation during the prior six months, and that the Gulf has essentially no 'memory' of longer (e.g., decadal) influences.

Regression between mean NSG salinity, and 192-day averaged net evaporation, indicated that a sustained change of $1x10^{-3}$m day^{-1} of net evaporation induced a salinity change of 0.23gl^{-1}. With averaged net evaporation as a proxy indicator of NSG salinity, the mean salinity of NSG during the period 1982-2009 was inferred to be 41.56gl^{-1}; the mean peak-to-trough annual variation was 1.38gl^{-1}; mean salinity shifted upwards by 0.77gl^{-1} during the ten year period to 2007/8 and, on average, the annual salinity maximum was reached on 12th April, and the minimum on 14th October.

Assuming that desalination (by removing freshwater) is equivalent to evaporation, the regression result was used to estimate potential desalination impacts on NSG salinities. The 'worst case' assumption in which all return water associated with an average desalination rate of 251 megalitres day^{-1}, is absorbed entirely within NSG, implies an increase of NSG salinity by up to $0.11gl^{-1}$, to a new mean of $41.67gl^{-1}$.

The effects of climate change on NSG salinity were similarly assessed by estimating changes of net evaporation from the projections of Suppiah et al (2006), implying increases of mean NSG salinity of up to $0.07gl^{-1}$ in 2030, and $0.22gl^{-1}$ in 2070. Combining these estimates of climate change and desalination impacts with the highest inferred salinity of the past 27 years (obtained from the net evaporation proxy), implies an upward shift of mean NSG salinity of $0.61gl^{-1}$ in 2030, and $0.76gl^{-1}$ in 2070 compared with the 1982-2009 mean.

Finally, the oceanographic mechanisms of salt discharge were examined in order to assess whether they may suffer irreversible disruption by anticipated perturbations associated with desalination and climate change. Regardless of which mechanism is primarily responsible for maintaining the long-term salt balance of NSG (that is, gravitational circulation or turbulent dispersion) each is expected to adapt smoothly, modestly and reversibly to anticipated disturbances.

1 Introduction

On 1 May 2009 BHP Billiton released the Olympic Dam Expansion Draft Environmental Impact Statement (BHP Billiton, 2009) detailing the proposal to expand its mining facilities and related infrastructure. Included within the planned development was a coastal desalination plant at Point Lowly in Upper Spencer Gulf which is required to yield an average of 251 megalitres day^{-1} of freshwater for the Olympic Dam expansion. In community discussion about the proposal, questions have been raised about the potential for significant long-term change of salinity in Upper Spencer Gulf, particularly when combined with anticipated effects of climate change.

This report addresses questions relating specifically to the long-term salt balance of Spencer Gulf. It does not address local-scale issues associated with the dilution and discharge of return water in the vicinity of the desalination plant itself. The purpose of this report is to examine the factors that are primarily responsible for determining the large-scale balance and distribution of salt in the Gulf, and to assess the potential for both natural and anthropogenic influences to perturb their extant character.

Based primarily on long-term measurement of salinity and environmental conditions, this report quantifies the relationship between natural evaporative forcing and salinity change in northern Spencer Gulf. Assuming (as discussed below) that desalination and climate change may be treated as perturbations of evaporation (freshwater removal) and precipitation, quantitative assessment of their separate and combined effects on the northern Gulf's salinity are derived.

1.1 Background and Context

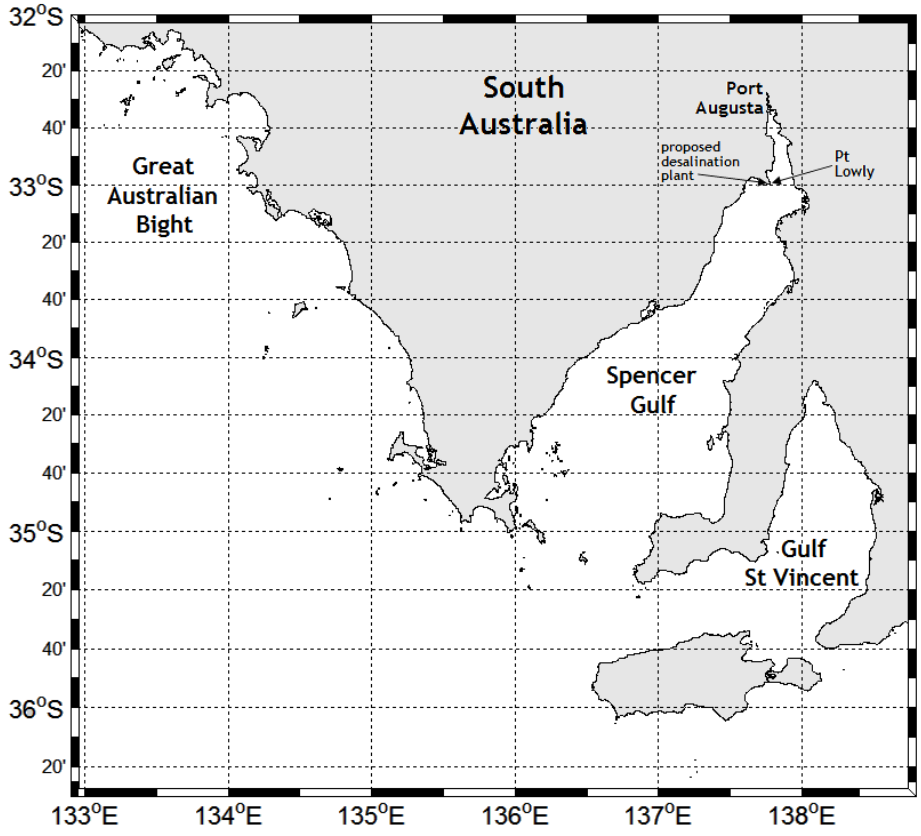

Figure 1. The South Australian Gulfs

Spencer Gulf (Figure 1) is an 'inverse estuary' (see for example, Bye, 1981; Nunes & Lennon, 1986, hereafter called NL86; and Nunes Vaz et al, 1990, hereafter called NV90), that is, a semi-enclosed sea in which seawater is measurably concentrated (rather than diluted, which is the case in a 'classical estuary') by the removal of freshwater due to evaporation. Annual mean salinity rises from values of approximately 36 grams per litre[1] (gl^{-1}) on the adjacent continental shelf, to more than $45gl^{-1}$ near the head of the Gulf, at Port Augusta. To avoid confusion with other studies, the area of Upper Spencer Gulf north of 33°S will be referred to as 'northern Spencer Gulf' (NSG), as identified in Figure 2.

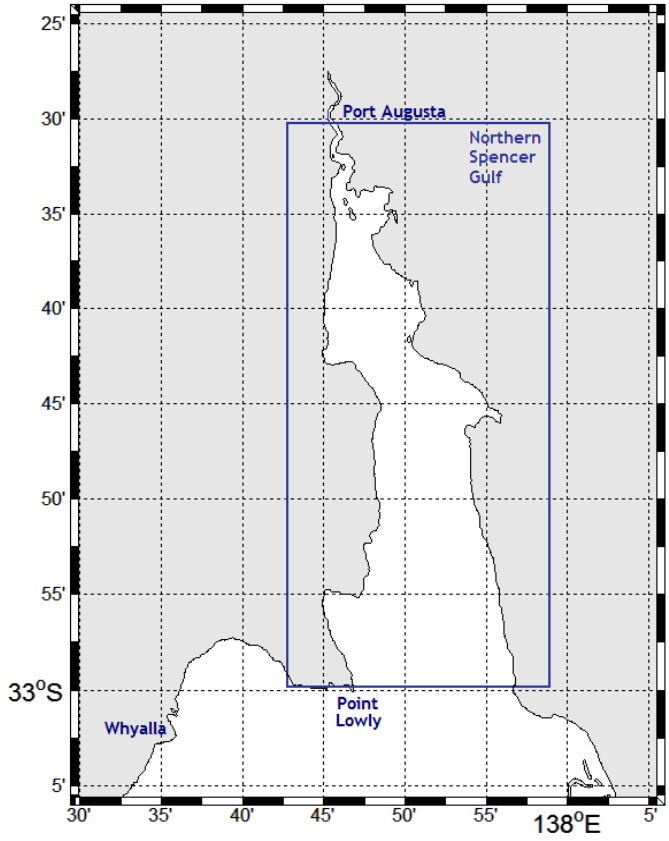

Figure 2. The area of interest, termed 'northern Spencer Gulf'

Figure 3 shows a simple schematic representation of Spencer Gulf and its one-dimensional fluxes of salt. Annual mean net evaporation[2] over the entire surface, removes freshwater which must be replaced by a net influx of seawater. This 'atmospherically-induced' landward salt flux is represented by S_a in Figure 3. It is the origin of the Gulf's elevated salinities or inverse estuarine character because the freshwater loss can only be replaced by seawater. Increasingly remote parts of the Gulf (equivalent to increasing distance from the ocean in this one-dimensional representation) are characterised by higher salinities, because the addition of salt is cumulative on moving north with the landward flow. The net effect is to create a one-dimensional salinity gradient along the Gulf with highest salinities at the head, as indicated in Figure 3.

[1] Despite the oceanographic convention which has now removed all reference to units, salinity will be expressed in units of grams per litre from here onwards, in keeping with parallel modelling and ecology reports associated with the BHPB desalination proposal.

[2] The cycle of net evaporation is negative at various times in the winter when precipitation exceeds evaporation but, averaged through the annual cycle, net evaporation is positive.

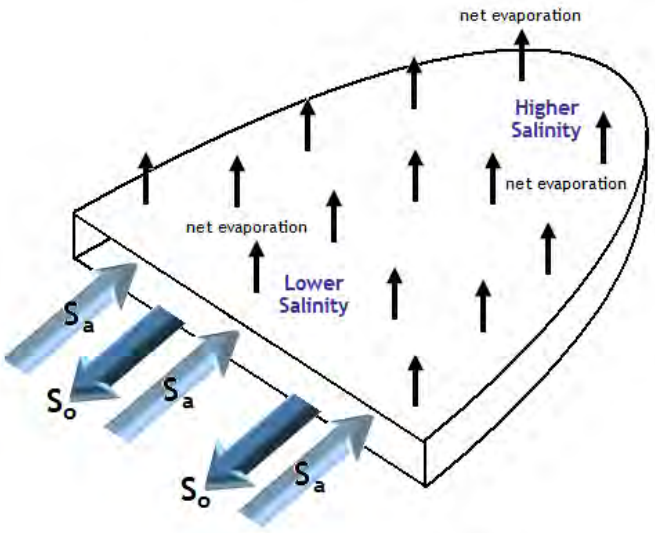

Figure 3. Schematic inverse estuary showing one-dimensional salt fluxes

If there were no other processes operating, the salinity of Spencer Gulf would continue to rise year after year (almost) without bounds. However, observations (and common experience) indicate that salinities do not continually rise, and this is because there is a net[3] seaward flux of salt of similar magnitude to the landward flux. The seaward salt flux is of 'oceanographic' origin, and is indicated as S_o in Figure 3. Precisely which oceanographic mechanisms generate the seaward salt flux is actually of little importance in this analysis, but a number of studies (for example, Lennon et al, 1987; NV90) have indicated that it is associated with the combined effects of turbulent dispersion, from internal shear and wind- and tide-induced stirring at the surface and seabed, and gravitational circulation driven by the horizontal gradients of density (largely due to salinity). Both turbulent dispersion and gravitational circulation always act to move salt down the salinity gradient, that is, from higher salinities to lower salinities. Thus, the oceanographic salt flux will always align itself to counter the effects of the landward flux due to net evaporation. It is also assumed[4], and examined in detail in section 6.6, that the seaward oceanographic salt flux is approximately constant all year round – to the same extent that the salinity gradient can also be considered approximately constant.

In addition to the mean salinity gradient, observations during the early 1980s (NL86) showed that there is an annual salinity cycle with an amplitude that increases from approximately $0.3gl^{-1}$ on the shelf to more than $5gl^{-1}$ near the head. The annual salinity cycle is delayed relative to the annual cycle of net evaporation. Salinity was seen to reach its annual maximum in early- to mid-March in northern Spencer Gulf (and not until early June at the mouth) compared with the net evaporation cycle which generally reaches its maximum in January. The lag of salinities behind the net evaporation cycle may be seen as a form of 'haline inertia', akin to the thermal inertia which causes the lag of Gulf temperatures behind the insolation cycle. The temperature lag due to thermal inertia also increases from less than

[3] annual mean

[4] Nunes-Vaz & Lennon (1987), for example, established that seaward salt flux in Spencer Gulf can be episodic, that is unsteady, showing a seasonal bias with maximum salt discharge tending to occur around autumn. The tendency to stratify and generate density outflows, and their resistance to turbulent destruction, however, were shown to be inversely related to water depth. Thus, the upper (shallower) parts of Spencer Gulf are expected to display a tendency to more frequent (daily to weekly, rather than seasonal) short-lived (of the order of 1 hour) discharge events, and therefore a relatively steady seaward salt flux compared with more southerly regions of the Gulf.

a month in the northern reaches of NSG to nearly three months at the mouth (see NL86 for details)[5].

In any single year (see Figure 4) there will be times when the landward salt flux (represented by the blue curve in Figure 4) is larger than its annual mean (during the summer months when net evaporation is relatively high) so that the magnitude of the landward flux exceeds that of the seaward flux (represented by the straight blue line in Figure 4). At these times, the Gulf accumulates salt, and salinities (red) show a rising trend. At other times of the year (particularly in winter), when the landward flux is less than its annual average, the seaward flux exceeds the landward flux and salinities fall. The net salt flux (magenta), due to the combination of the two influences shows an annual cycle with a mean close to zero.

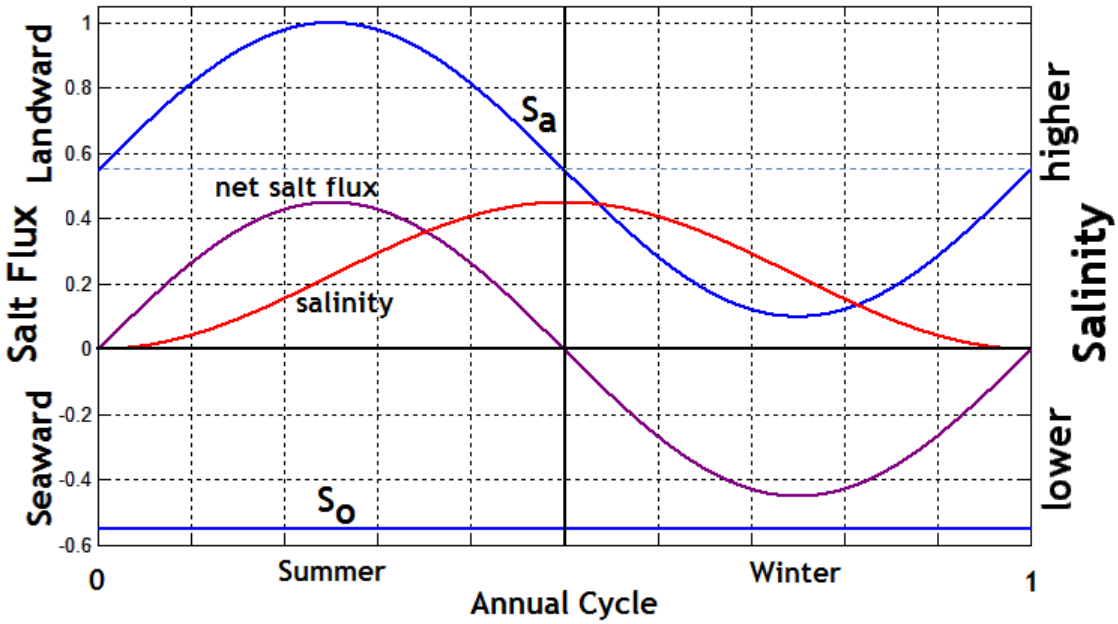

Figure 4. Representation of one-dimensional salt fluxes in Spencer Gulf. The flux of salt induced by evaporation (blue curve) has a positive (landward) mean which is balanced by an equal negative (assumed constant) seaward flux (blue line) caused by various oceanographic exchange processes discussed in the text. The net flux of salt (purple), which is positive in summer and negative in winter (with a mean of zero), causes a salinity cycle (red) that lags the salt flux cycle, causing maximum salinity to occur later than the peak of evaporation.

On a long-term basis, the landward 'atmospherically-induced' salt flux is approximately balanced by the seaward 'oceanographic' salt flux so that the mean salinity of Spencer Gulf varies only modestly according to the slight, interannual imbalance between the two influences. Why is this so – why are the two influences approximately balanced? The strength of the seaward salt flux, whether generated by turbulent dispersion or gravitational circulation, is related to the mouth-to-head salinity gradient. If net evaporation were to increase for a sustained period, this would enhance the landward salt flux, S_a, causing both

[5] It is interesting to note (NV90; Petrusevics, 1993; and Whitehead, 1998) that the natural decline of the longitudinal salinity gradient from the head to the mouth, permits summertime temperature gradients to switch the Gulf from its inverse estuarine character to classical estuarine character in the vicinity of the mouth. Its effect is to block the discharge of accumulated salt for a month or two during summer, but this arrangement is necessarily broken during the cooler months when longitudinal gradients of temperature reinforce those of salinity allowing the Gulf to freely exchange salt with the adjacent shelf.

the salinity at the head and the along-Gulf salinity gradient, to increase which, in turn, would increase the seaward (counter) flux. This negative feedback system produces a long-term stable equilibrium in which the mean magnitude of the salinity gradient, driving the seaward flux, adapts to the mean strength of the landward flux.

However, three questions remain with regard to the Gulf's equilibrium dynamics, which this report aims to answer, namely:

1. how rapidly Spencer Gulf responds to influences that disturb its salinity, and how long it takes to 'recover' following a disturbance?
2. the degree or extent to which salinity is expected to change in response to a disturbance, and
3. whether anticipated perturbations associated with desalination and climate change will be large enough to shift the Gulf's salinity, irreversibly, to a new equilibrium state.

In answering these questions, the recent history (1982 to 2009) of precipitation and evaporation is first examined to understand mean atmospheric forcing, and the extent of any significant trends. The salinity response of northern Spencer Gulf is then examined over the same 27-year period, to determine the nature of the relationship between forcing and response. Once 'calibrated' in this way, expected perturbations of mean NSG salinity due to desalination and climate change are derived, followed by a theoretical assessment of the dynamics of the seaward salt flux and whether it may be over-stressed by (and possibly unstable to) anticipated changes.

2 Long-Term Data Trends and Relationships

2.1 Atmospheric Influences

The Bureau of Meteorology operates many data collection stations in South Australia. However, the regularity and longevity of these records vary substantially which means that very few are potentially useful to this study. Figure 5 shows the locations of four stations (Ceduna, Spalding, Price and Adelaide Airport), closest to Spencer Gulf, for which records span the period 1982 to 2009, and for which both precipitation and evaporation were measured.

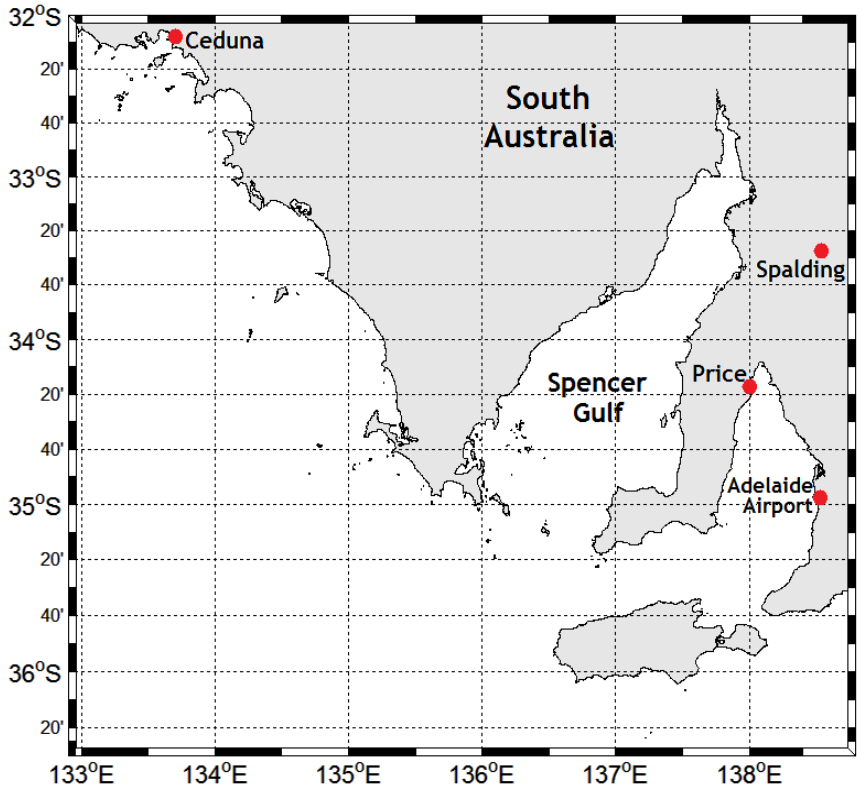

Figure 5. Adelaide Airport, Price, Spalding and Ceduna meteorological stations providing long-term records of precipitation and evaporation.

Evaporation measurements reported by the Australian Bureau of Meteorology are unadjusted US Class A Pan Evaporimeter measurements, representing the measured daily loss of water from a metal pan of standard dimensions. Discussion of the interpretation and adjustment of pan evaporation data is held over until section 2.1.1 below, but for the purposes of this report, pan evaporation multiplied by a factor (called the pan factor or pan coefficient, see Hounam, 1973) of 0.7 – called 'adjusted evaporation' - is used as a long-term proxy indicator of environmental evaporation.

Net evaporation is evaluated as adjusted evaporation minus precipitation (measured in millimetres day^{-1}). Figure 6 shows the daily, net evaporation data for the four stations, plotted on equivalent vertical scales.

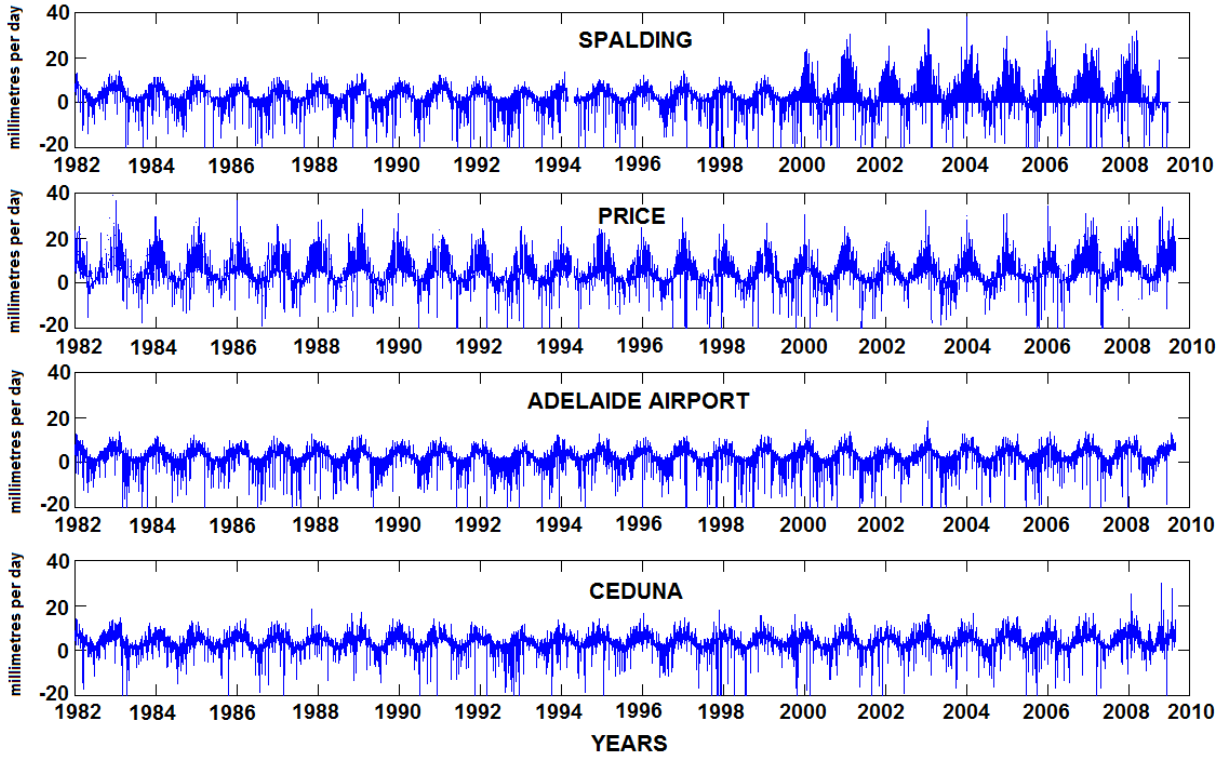

Figure 6. Daily net evaporation at Spalding, Price, Adelaide Airport and Ceduna stations

From approximately 2000 onwards, data from Spalding show anomalous behaviour, suggesting that Spalding may not provide long-term data of suitable quality.

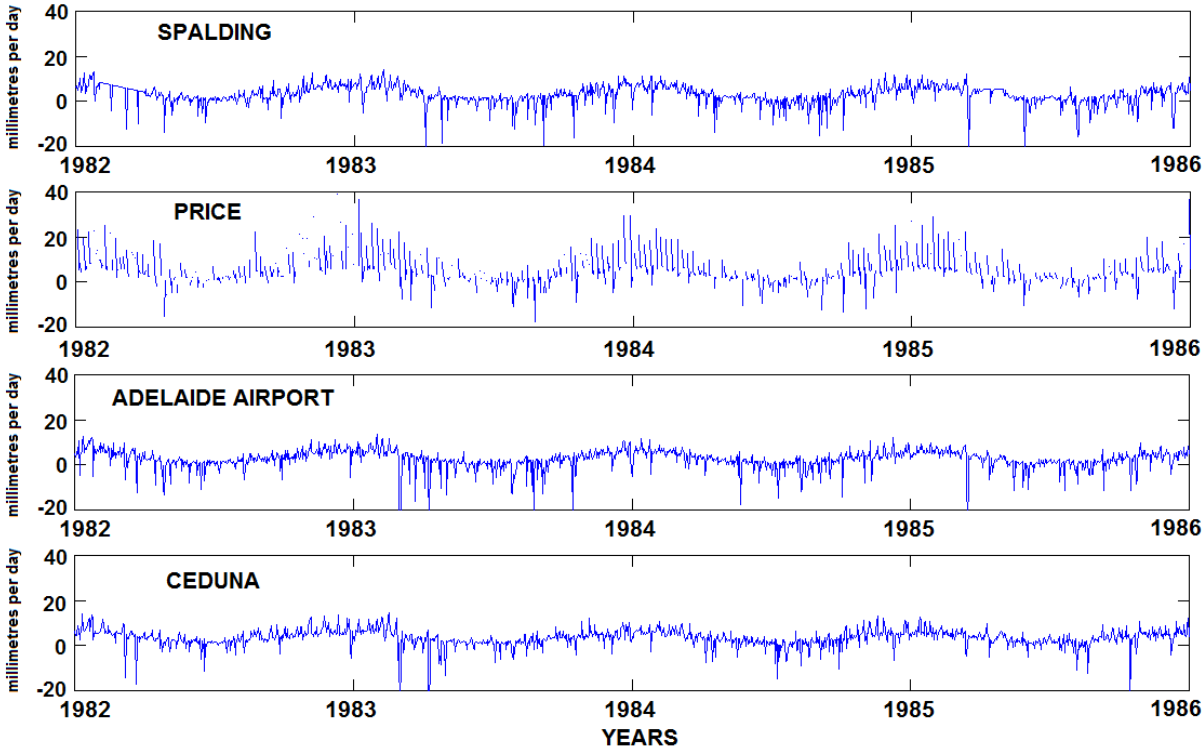

Figure 7. Daily net evaporation at Spalding, Price, Adelaide Airport and Ceduna stations

Figure 7 shows the same data plotted for the shorter period 1982 to 1986, exposing the fact that the Price record has a great many missing data points, which is the case throughout the

record. In fact the missing data reflect a different data collection regime whereby several days (usually including weekends) may elapse before another reading is taken. Replacing all missing data with zeros provides a dataset that is useful for assessing long-term averaged behaviour, smoothing out the large day-to-day fluctuations.

A running mean for any dataset may be calculated as follows. The running mean has a filter or window length which describes the span of the data it assesses. For a 1-year (365-day) running mean, 365 daily values are read in, the mean is calculated and the value is assigned to a particular day. For a central running mean, the algorithm takes a data point together with 182 points from either side, and assigns the mean of all 365 values to the central point. It then moves to the next point and repeats the process. A 365-day central running mean cannot be evaluated until the 183rd data point from the start of the dataset, and similarly it yields no results for data closer than 183 data points from the end. Thus the filter produces a result which is half the filter length short at each end (for a centralised filter).

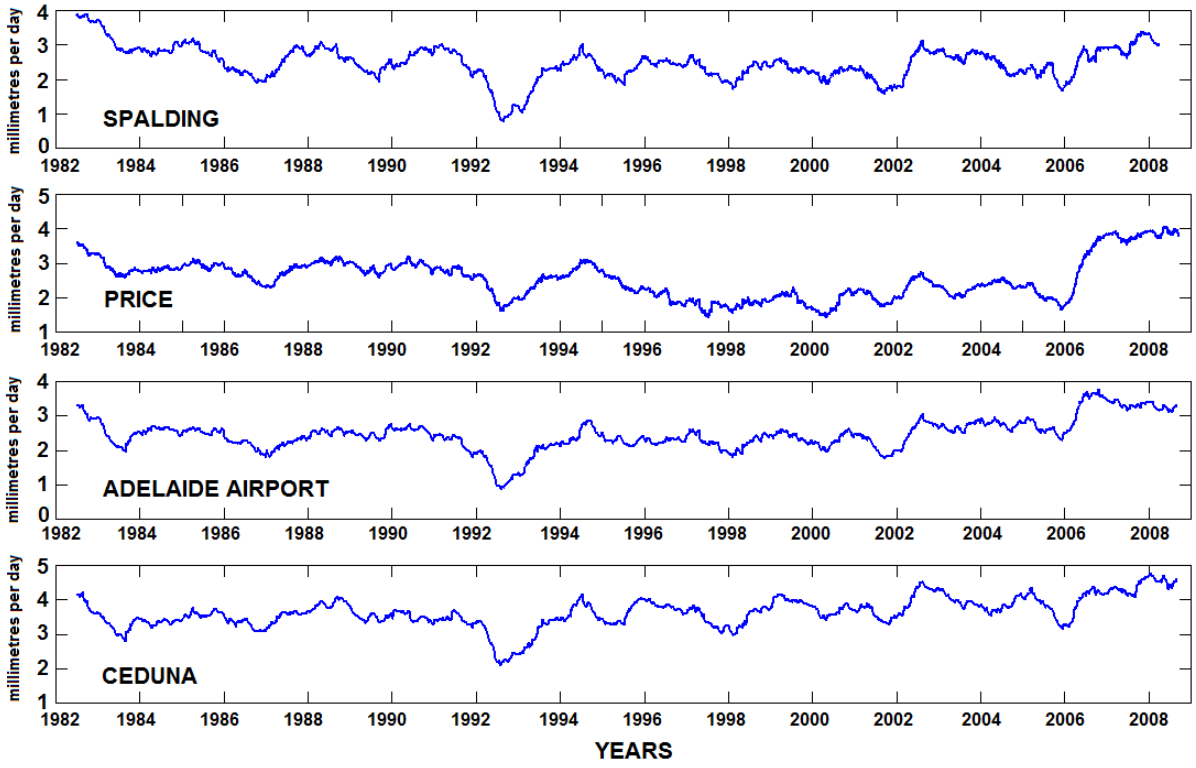

Figure 8. One-year running means of net evaporation at Spalding, Price, Adelaide Airport and Ceduna. Missing data points in the Spalding and Price records shown in Fig 7, were filled with zeros.

Figure 8 shows the result of this process applied to the four net evaporation datasets. All filtered results are visually correlated (more easily seen in figure 9) which is encouraging with regard to data quality. Note that all records indicate increased net evaporation in the late 2000s, but Price shows a very marked change not duplicated at Spalding (the closest station to NSG).

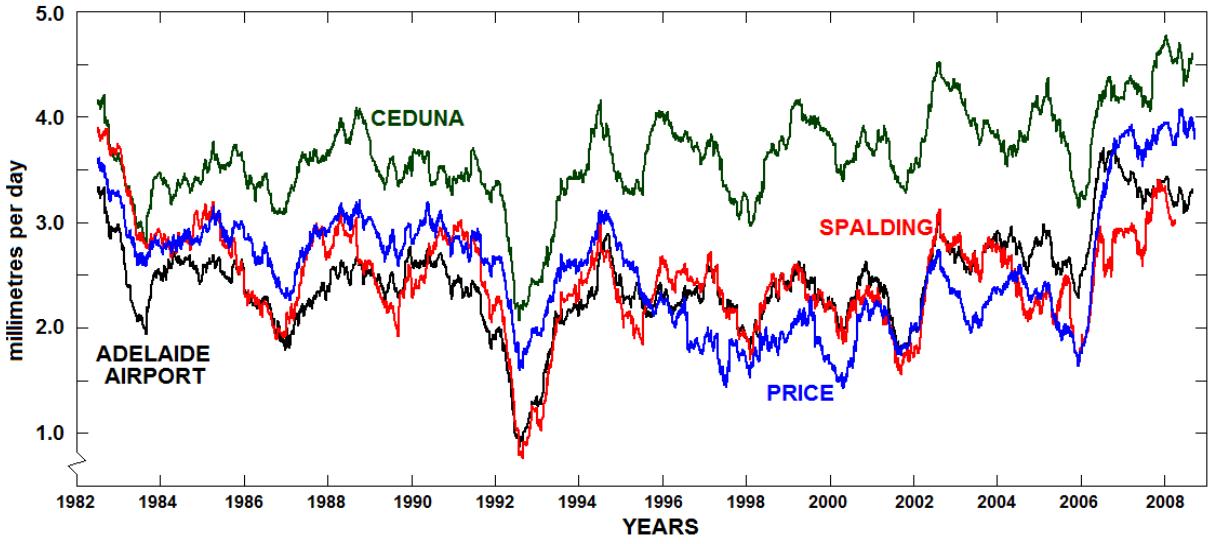

Figure 9. One-year running means of net evaporation at Spalding, Price, Adelaide Airport and Ceduna stations

Figure 9 indicates that there was significant agreement between net evaporation data at Adelaide Airport, Price and Spalding, while the Ceduna record showed similar interannual structure around a substantially higher mean. Due to the high-frequency incompleteness of the Spalding and Price records, their filtered results show significantly more noise. The following analysis will focus on Spalding, Price and Adelaide Airport records, as Ceduna appears to show disparate behaviours compared with the three stations closest to northern Spencer Gulf.

Figure 10 shows the long-term trends of atmospheric forcing, that is, precipitation, adjusted evaporation and net evaporation for Adelaide Airport for the entire 1982 to 2010 period, as 1-year, 3-year and 5-year central running means. Note that the y-axis scale range is the same for precipitation (shown as negative) and evaporation, but these differ from the scaling used for net evaporation (which has a larger range).

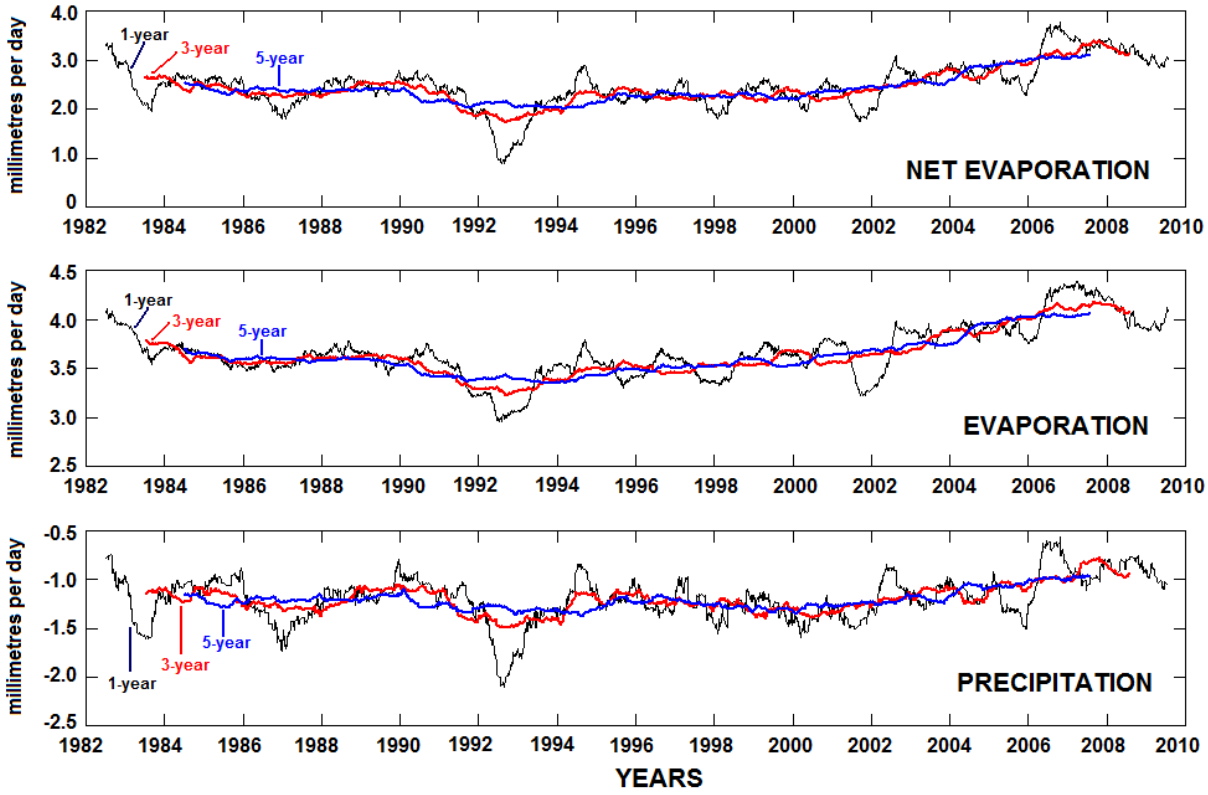

Figure 10. 1-year, 3-year and 5-year running means of meteorological data from Adelaide Airport

From the early 1980s net evaporation at Adelaide Airport, which shows significant inter-annual variability, experienced a downward trend until the mid-1990s and, since that time has risen to levels above those of the early 1980s. The downward trend is consistent with the averaged behaviour of all Australian Class A pans from the early 1980s (Gifford et al, 2005; Roderick et al, 2009). Gifford et al (2005) are ambiguous in describing trends after the mid 1990s, although they do state that from 1994 "… the data for Australia have shown a slowdown and reversal of the downward trend especially in the eastern part [of Australia]…". This is consistent with the data for Adelaide Airport (and Price and Spalding), where net evaporation has risen consistently for more than a decade, and may still be rising (according to the 5-year running mean).

The trends of Adelaide Airport net evaporation are evident in both precipitation and evaporation data (precipitation is plotted on a negative scale to make the addition with evaporation visually simpler). The long-term trend of increasing evaporation was accompanied by decreasing precipitation (and vice versa). This correlation, which is commonly seen in such data (Gifford et al, 2005), extends well into shorter period fluctuations.

These conclusions are also consistent with the behaviour of meteorological data from Spalding and Price stations.

2.1.1 Extrapolating Pan Evaporation to Evaporation from Northern Spencer Gulf

Much has been written about the validity or otherwise of using data from US Class A Pan Evaporimeters to infer environmental evaporation rates (see for example, Linacre, 2005). Evaporation pans suffer from many sources of error (Linacre, 2005) including algal growth, shade or wind shelter due to trees and buildings, the changing albedo of sediment, animal or

bird drinking (although mesh guards are generally used nowadays), heat applied to the sides of the pan from direct and diffuse radiation, and both short-wave reflection and long-wave radiation from the changing surrounds.

However, despite these difficulties, pan evaporation provides data which is generally consistent with the Penman equation, which predicts potential evaporation based on daily mean temperature, wind speed, relative humidity and solar radiation, and with measurements of 'lake evaporation', determined by water balance methods where the lake is "small and shallow enough to have no horizontal or vertical currents nor to alter appreciably the atmosphere above it" (Linacre, 2005). Such correlations improve when considering longer-term averaged data, such that Johnson & Sharma (2007) obtained a correlation of 0.97 between monthly means of pan evaporation and evaporation inferred from the Penman equation.

Comparison between evaporation measured using Class A pans, and estimates from mass balance calculations in lakes, and from the Penman equation indicate that Class A pans over-estimate evaporation, in general because pans are subject to additional heat effects through their sides. For this reason, a correction factor, called the pan factor or pan coefficient, is commonly applied to pan evaporation measurements in order to estimate the evaporation which is expected to occur from small water bodies such as lakes. Estimates of pan coefficients vary from 0.7 to 0.8 according to context and dataset, however, Linacre (1994), in Australian conditions, found that lake evaporation is approximately 0.7 times the evaporation from a Class A pan.

Evaporation from the oceans is not well represented by evaporation from Class A pans (Farquhar & Roderick, 2005), firstly because their thermal inertias are very different, that is, the oceans' ability to absorb heat without appreciably changing its temperature means that the pan is not a good model of oceanic heat budgets, and secondly because a marine boundary layer forms over large bodies of water, which greatly modifies properties, such as humidity, that play a large role in driving evaporation. Thus pan evaporation from South Australian meteorological stations is not expected to provide a valid proxy indicator of evaporation from, for example, South Australian shelf waters.

However, the upper part of Spencer Gulf, north of 33°S is a relatively narrow and shallow water body. A significant fraction of its evaporation is anticipated to occur around its margins where thermal inertia is relatively small and diurnal temperature changes are significant. Furthermore, a marine boundary layer may remain undeveloped for all but winds with predominantly southerly or northerly components, although these are the dominant winds in summer.

Thus, although evaporation inferred from Class A pans remains an imperfect proxy measure of evaporation from northern Spencer Gulf, it is expected that it should provide useful insights into properties that are significantly influenced by evaporation. On the basis of such caveats, the analysis proceeds using evaporation measured by Class A pan evaporimeter, adjusted using a pan factor of 0.7, as an indicator of evaporation from northern Spencer Gulf: a value at the low end of the normal range of pan coefficients because this will exaggerate or lead to upper-bound estimates of the potential environmental (and desalination) effects on NSG.

2.2 The Salinity Response of Northern Spencer Gulf

Nunes Vaz (1985) and NL86 reported the results of fourteen large-scale three-dimensional surveys of temperature and salinity in Spencer Gulf from mid-1982 to early 1985. These surveys (using an internally-recording Applied Microsystems electronic conductivity-

temperature-depth, or CTD, probe) profiled conditions at many stations between the head and points as far south as 34° 20'S.

In NSG, where salinities often rise above the measurable limit ($42 gl^{-1}$) of typical oceanographic instrumentation, a perspex sleeve was inserted into the probe's inductive cell to reduce the cell's sample volume and thus reduce its sensitivity, to bring the highest salinities within measurable range. This practice destroyed the manufacturer's calibration between actual and measured salinity and, for this reason, both surface and bottom samples were collected (using Nansen or Niskin bottles) at every station, for measurement back in the laboratory using an accurate bench salinometer.

When measuring salinity using the (Yeokal) bench salinometer (actually measuring temperature, and conductivity ratio relative to a precisely known seawater standard), it was necessary to dilute the samples using a precisely known amount of de-ionised water, in order to lower the salinity below $42 gl^{-1}$, again into measurable range. Once determined, the measurement was adjusted upwards according to the amount of dilution. These samples consequently provided a separate multi- (typically 50-plus) point calibration of each CTD survey. Twelve such surveys provided substantial data in NSG during the 1980s.

Two further surveys of NSG were conducted on 6 August 2008 and 2 March 2009 (the data are provided in Appendix A). However, a profiling CTD probe was unavailable, and so salinity at each station was sampled using only near-surface and near-bottom water samples collected using a Nansen bottle. Nevertheless, the samples were analysed at Flinders University using the same bench salinometer as the analyses conducted in the 1980s. New salinity standards were shipped[6] from the UK and a cross-check was performed between the new standards, and three of the glass-sealed salinity standards shipped from the UK in the 1970s: the same batch of standards used to reference the analyses of NSG salinity at Flinders University during the 1980s. This inter-calibration showed that the 1970s standards had not measurably drifted, and permitted the new surveys to be precisely referenced to the 1980s data (to within $< 0.01 gl^{-1}$), making the whole long-term dataset particularly valuable in this regard.

In order to understand the salinity response of NSG as a whole, rather than assuming that repeated measurement at a single point in some way represents the behaviour of the whole body of NSG, the mean NSG salinity (or MNSGS) was derived from survey data as described in the following paragraphs.

[6] OSIL UK, http://www.seawatersolutions.com/index.asp

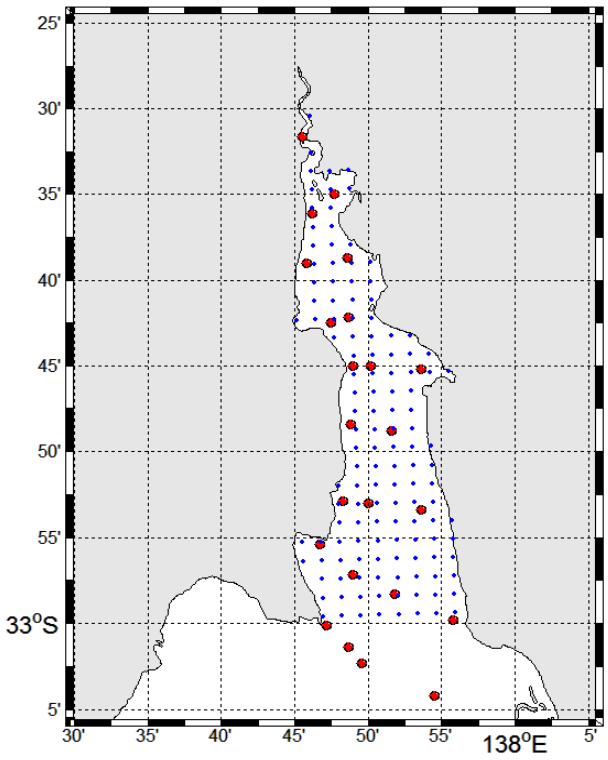

Figure 11. Northern Spencer Gulf with November 1982 survey stations (red circles) and a 2km by 2km interpolation grid (blue dots).

Figure 11 shows the location of stations in NSG from a typical survey, in this case 24th November 1982. For any particular survey such as this, the detailed vertical profile of salinity at each station yielded a depth-averaged salinity, and thus all stations in the survey allowed the region to be contoured for horizontal depth-averaged salinity. Using these contoured distributions, salinities were then interpolated or extrapolated onto the regular (2km by 2km) grid, shown in Figure 11 as blue dots. At each grid point, the mass of salt (that is, the interpolated salinity multiplied by the depth, then multiplied by $4km^2$) was determined, and summed for all (130) grid points. This salt mass was then divided by the mean depth of all grid points (and also $4km^2$) to give the mean salinity of NSG. This method was then repeated for all other surveys of NSG. Mean salinities calculated in this way are collected in Table 1.

#	SURVEY DATE	MEAN SALINITY
1	28 Jul 1982	$42.04gl^{-1} \pm 0.05gl^{-1}$
2	24 Nov 1982	$41.67gl^{-1} \pm 0.05gl^{-1}$
3	15 Jan 1983	$41.92gl^{-1} \pm 0.05gl^{-1}$
4	9 Feb 1983	$42.21gl^{-1} \pm 0.05gl^{-1}$
5	20 Apr 1983	$\mathbf{42.57}gl^{-1} \pm 0.05gl^{-1}$
6	22 Jun 1983	$41.68gl^{-1} \pm 0.05gl^{-1}$
7	11 Aug 1983	$\mathbf{40.90}gl^{-1} \pm 0.05gl^{-1}$
8	1 Nov 1983	$40.99gl^{-1} \pm 0.05gl^{-1}$

9	6 Mar 1984	$42.33 gl^{-1} \pm 0.05 gl^{-1}$
10	26 Jun 1984	$42.04 gl^{-1} \pm 0.05 gl^{-1}$
11	10 Oct 1984	$41.04 gl^{-1} \pm 0.05 gl^{-1}$
12	23 Jan 1985	$41.57 gl^{-1} \pm 0.05 gl^{-1}$
23 year gap		
13	6 Aug 2008	$41.97 gl^{-1} \pm 0.08 gl^{-1}$
14	2 Mar 2009	$42.70 gl^{-1} \pm 0.08 gl^{-1}$

Table 1. Mean salinities of NSG determined according to the method described in the text. Minimum and maximum values from the 1980s surveys are highlighted in boldface type.

Estimation of the error associated with the mean salinity from 1980s surveys was determined by adjusting the arrangements of salinity contours to the highest salinity (contours moved as far south as possible) and lowest salinity (contours moved as far north as possible) distributions using non-linear interpolation, while remaining consistent with the measured data. The mean salinity was then calculated from each extreme in the usual way, giving highest and lowest estimates for each survey.

The error associated with estimates of mean NSG salinity from the 2008 and 2009 surveys was larger than that of the 1980s because the data lacked information about the depth variation of salinity at each station. For this reason, one extreme arrangement of salinity contours was derived by assuming that the higher of the surface and bottom salinities at each station applied to the whole depth, and contours were pushed as far south as possible consistent with the station data, leading to the highest estimate of NSG mean salinity. The other extreme involved assuming that the lower of surface and bottom salinities applied to the whole depth at each station, and contours were pushed as far north as possible consistent with data, giving the lowest mean salinity estimate.

Figure 12 shows the 30-month variation of NSG mean salinity with a cubic spline fit to the data. Figure 13 enables more direct comparison, giving a sense of the inter-annual variation of the seasonal salinity response of NSG during 1982/83 (blue), 1983/84 (green) and 1984/85 (magenta). The late-summer maxima in April 1983 and March 1984 were similar, even though they were preceded by very different winter/spring minima. The minimum observed in 1982 was substantially higher than that of 1983, with the minimum of 1984 lying between the two.

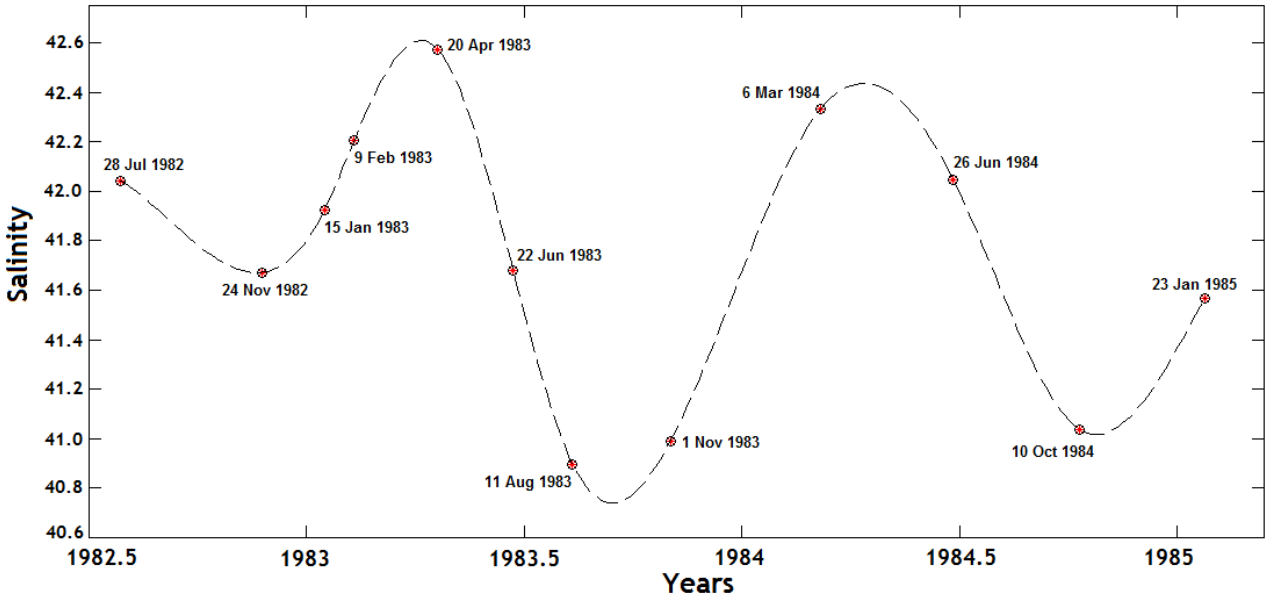

Figure 12. The variation of mean NSG salinity throughout the 30-month period of detailed measurement

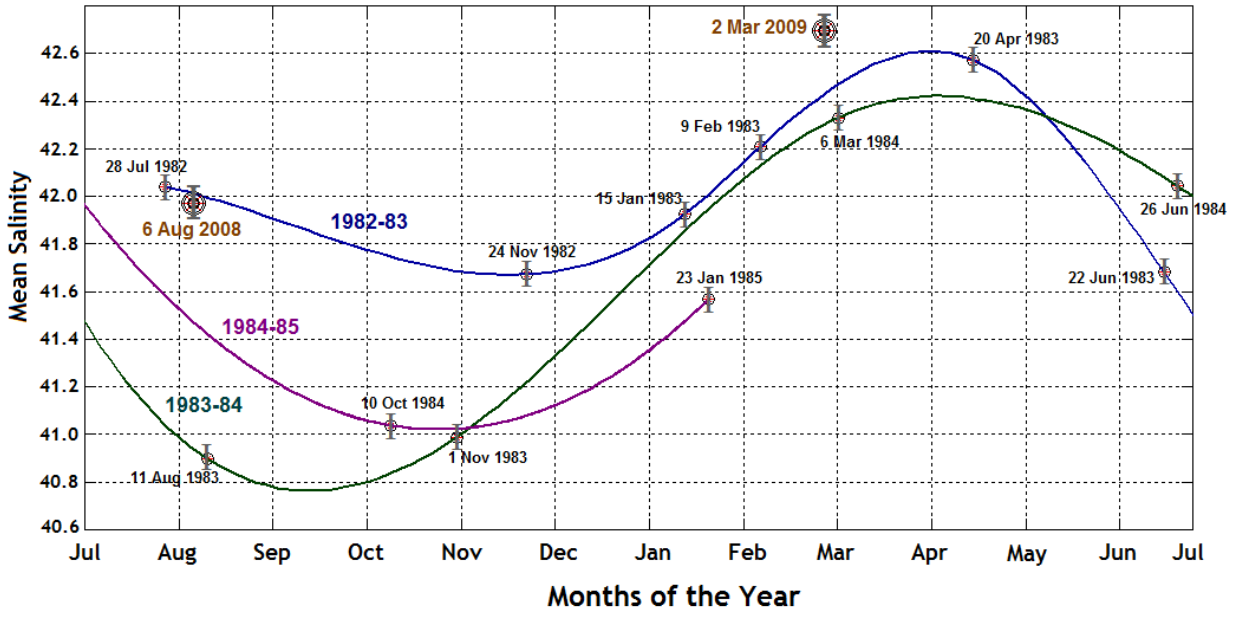

Figure 13. The mean salinity of NSG as separate annual cycles overlain for ease of comparison

The mean salinity of NSG based on 2 March 2009 data (42.70gl^{-1}) was the highest of the fourteen-survey, 27-year dataset, although it was only 7.8% outside the salinity range (40.90gl^{-1} to 42.57gl^{-1}) seen in the early 1980s. The mean salinity of 6 August 2008 lay within the variations seen at similar seasonal timings in the 1980s. Thus, the recent data could not be interpreted as in any way anomalous when referenced against 1980s data, although this interpretation is subject to potential revision awaiting assessment of atmospheric forcing, and its influence over equivalent periods. This is the subject of the next section.

3 The Relationship Between Atmospheric Forcing and the Salinity Response of Northern Spencer Gulf

The arguments of section 1 imply a hypothesis which may now be tested. The hypothesis can be stated as follows:

> *the mean salinity of northern Spencer Gulf reflects, in a consistent measurable way, the integrated influences of net evaporation during a preceding period whose length may be determined*.

In other words, anomalously high and sustained net evaporation is expected to raise salinities in NSG relative to mean behaviour. Similarly, sustained lower net evaporation is expected to lead to lower NSG mean salinities, noting that the meaning of 'sustained' must also be examined.

The hypothesis implies that the salinity on any particular day (say 'day-n') reflects the cumulative effects of net evaporation for 'x' days preceding day-n. Unlike the central running mean filter, a lagged filter is now required: one that averages x-days of net evaporation data, and assigns the result to the final day of the data window. The filter then moves forward one day and repeats the process, continuing to the end of the dataset.

Figure 14 shows raw (daily) net evaporation data from Adelaide Airport during the early 1980s (light blue, highly variable dataset), together with data obtained using a 90-day central running mean filter (dark blue), a 90-day lagged mean filter (magenta) and a 180-day lagged mean filter (red). Notice that the 90-day central running mean, and 90-day lagged filter series are identical (as they should be) except for a 90-day relative shift along the time axis. Note also that the longer the filter, the smoother the data, and the smaller the range. For lagged filters, all of the data loss associated with the filter length occurs at the beginning of the dataset, which is why each filtered result starts on a different day.

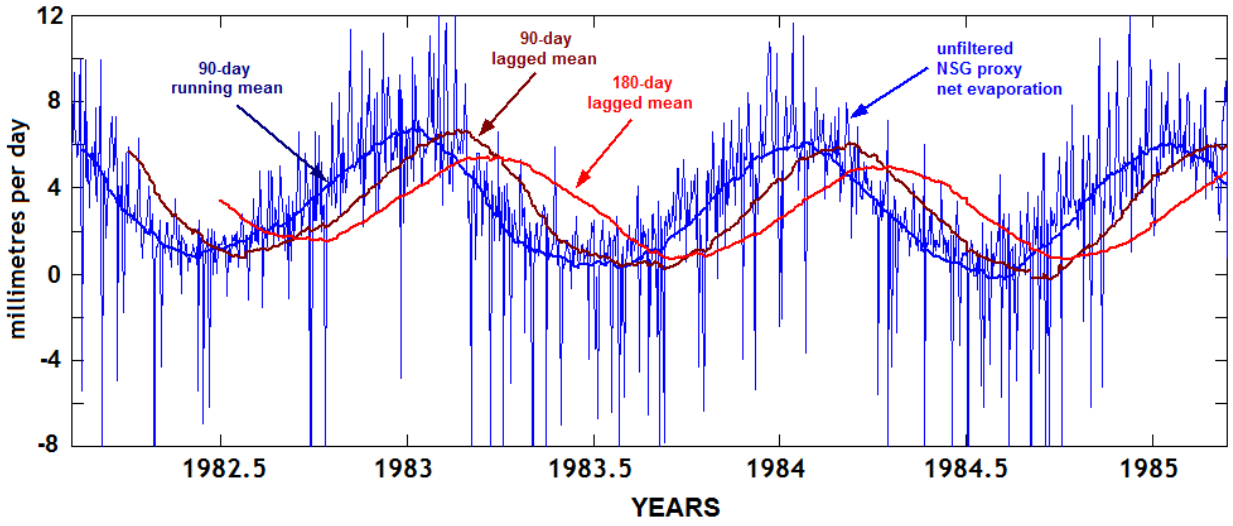

Figure 14. NSG proxy net evaporation, with various filtered derivatives

In order to compare 'lagged mean net evaporation' (LMNE) with mean NSG salinity (MNSGS), both datasets must be normalised (re-scaled to a range from zero to one) so that they can be plotted on the same axes. The assessment of the relationship between net evaporation and salinity response initially focuses on the 1980s data alone, so that data from the more recent surveys may be reserved as independent tests of any inferred relationship. Mean NSG salinities were normalised using the minimum (survey #7 of Table 1) and

maximum (survey #5 of Table 1) measured values. Similarly, after filtering net evaporation data, the result was normalized using the minimum and maximum LMNE observed within the same period.

Figure 15 shows normalised lagged mean net evaporation using six different filter lengths (90 days up to 208 days) plotted with normalised mean NSG salinity. A filter length of 208 days was the maximum that could be applied without losing the ability to compare with the first salinity data point which was obtained 209 days into 1982.

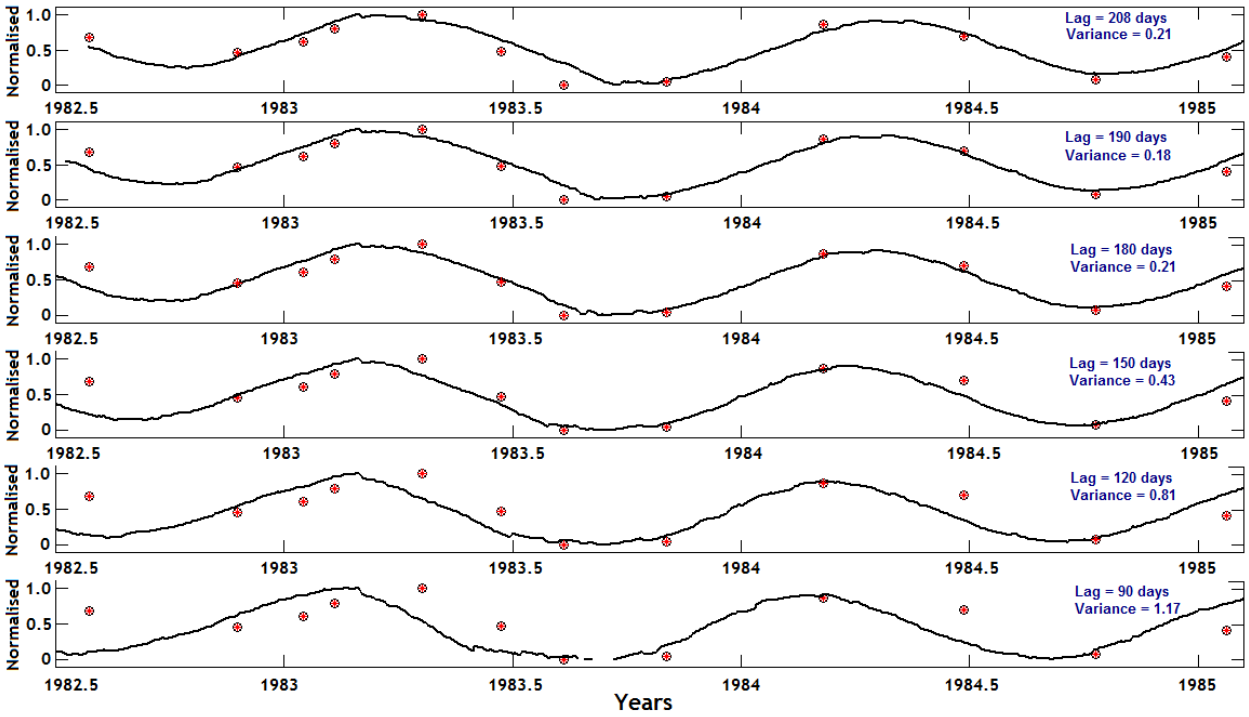

Figure 15. LMNE (black line) at Adelaide Airport versus MNSGS (red data points: see text) for various different filter lengths

The variance (sum of the squared differences between the discrete salinity data points and the specific values of LMNE on equivalent days) is also shown in each of the plots of Figure 15. By varying the lag period one day at a time, the variance was seen to follow a broad minimum for lagged filter lengths between 190 days and 200 days, with the optimum lag at 190 days.

Figure 16 shows the filtered results using optimum lags from each of Adelaide Airport (lag of 190 days), Price (192 days) and Spalding (192 days), and their variances, fitted to the 1980s NSG salinity results. The result with the smallest variance (0.16) was obtained using net evaporation from Price, although all three results are similar.

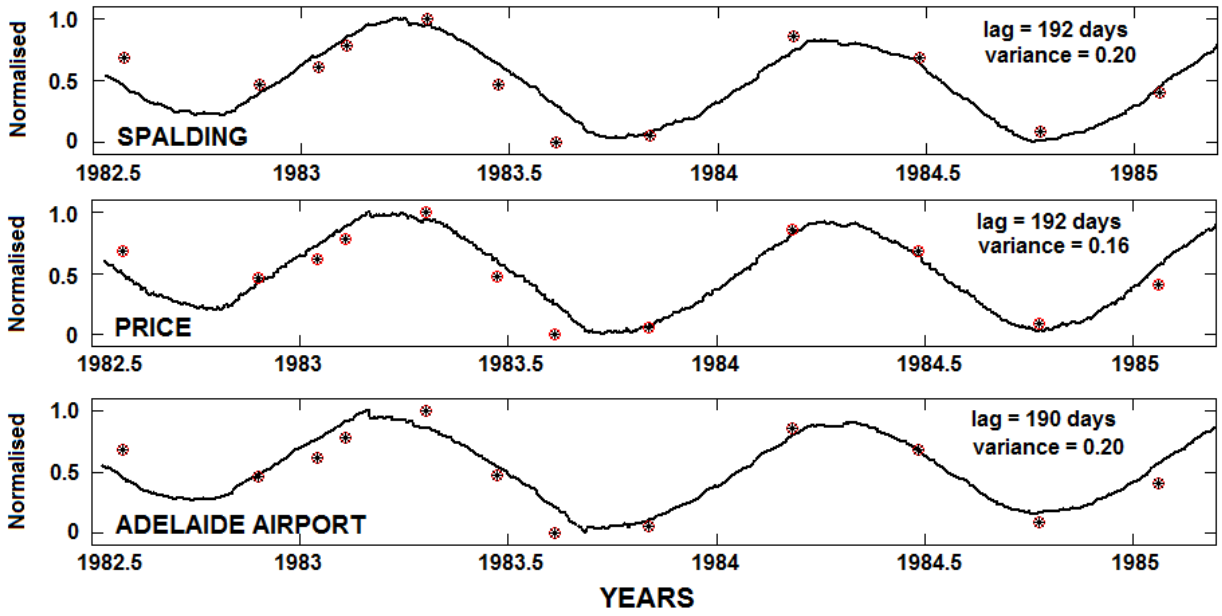

Figure 16. LMNE (solid lines) from Adelaide Airport, Price and Spalding stations, for lags that achieve the smallest variance when fitted to MNSGS data (discrete points). The optimum filter lag, in days, is indicated on each panel, together with the corresponding variance.

The message from these results is significant: that, at least during the 30-months of observations in the early 1980s, the mean salinity of NSG on any particular day closely reflected the accumulated effects of net evaporation during the preceding 190 or 192 days (approximately six months). This goes some way to answering the question about the response timescale of NSG: it suggests that the Gulf largely responded to variations of less than annual period, although this limited (30-month) dataset is not definitive with respect to longer-term (decadal) influences.

Figure 17 provides a different view of the same data shown in Figure 16. Note that the inter-annual differences between the maxima of 1983 and 1984 have the same sense as the changes in observed salinity in the same years. Similarly, the minima of LMNE in 1982, 1983 and 1984 mirror the changes in the depth of the salinity minima (other than Spalding for 1983 and 1984).

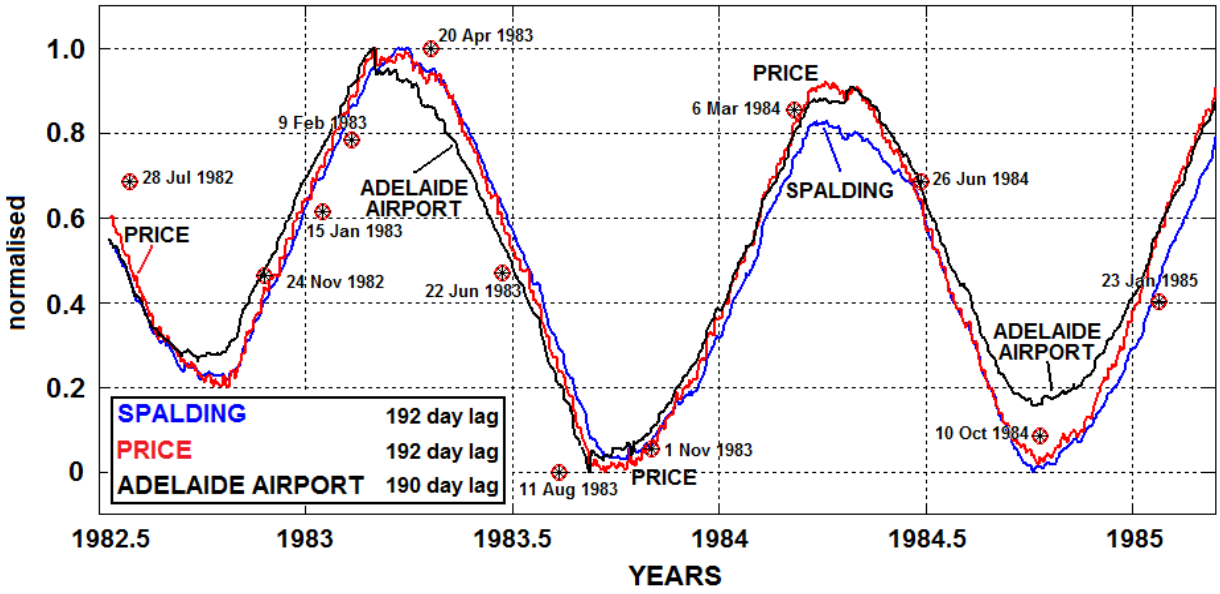

Figure 17. LMNE from Adelaide Airport (black), Price (red) and Spalding (blue), for lags that achieve the smallest variance when fitted to MNSGS data (discrete points).

3.1 The Long-Term Behaviour of Northern Spencer Gulf

Results discussed above suggest that NSG salinity on any particular day was determined, to a significant degree, by the cumulative effects of net evaporation during the preceding six months. The question remains, however, as to whether there is a longer-term component of the response that accumulates the effects of much lower frequencies in the forcing, which might drive significant shifts of mean NSG salinity.

Given that net evaporation sustained a consistent increasing trend for more than a decade (Figure 10), if NSG salinity is sensitive to the longer-term rising trend then extension of the simple 1980s 'six-month memory' relationship, should reveal whether a shift of the mean salinity datum has occurred.

Figure 18 shows this result using net evaporation from Price. It was constructed by continuing the 192-day lagged mean filter for net evaporation, and maintaining the normalisation used for the 1980s data, that is, both MNSGS and LMNE were normalised to the early-1983 summer maximum and late-1983 winter minimum.

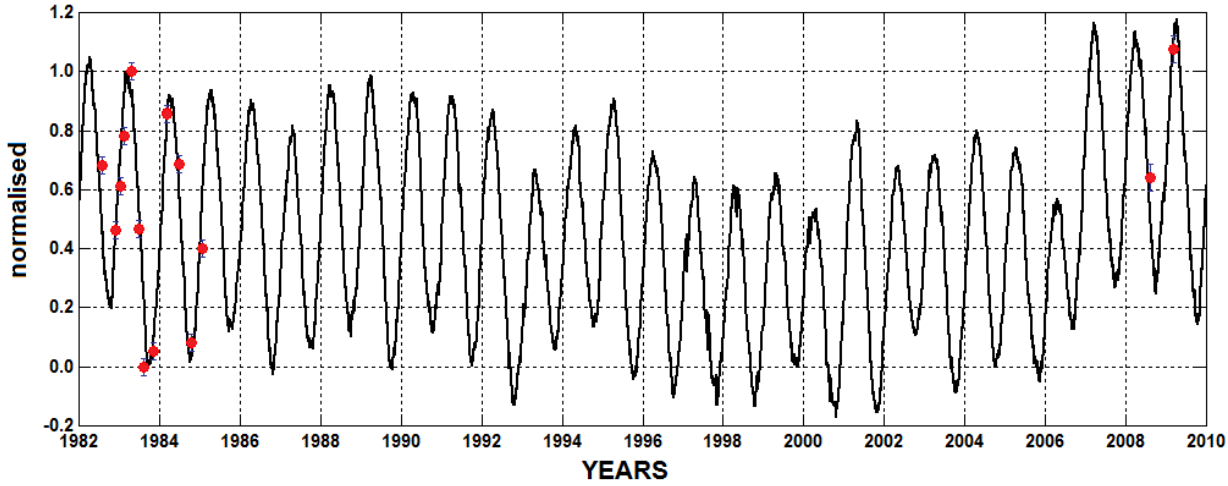

Figure 18. LMNE for Price (solid), using 192d lag and the same 1980s normalisation established above, extended through to 2009, compared with the full MNSGS dataset (discrete points with error bars).

Figure 19 shows the results of Figure 18 re-plotted to include only those years when observations of salinity were made. Again, the Figure was not re-scaled or re-normalised, and thus the upward shift of observed NSG salinity between 1980s and late 2000s data is mirrored in the upward shift of lagged net evaporation measured at Price.

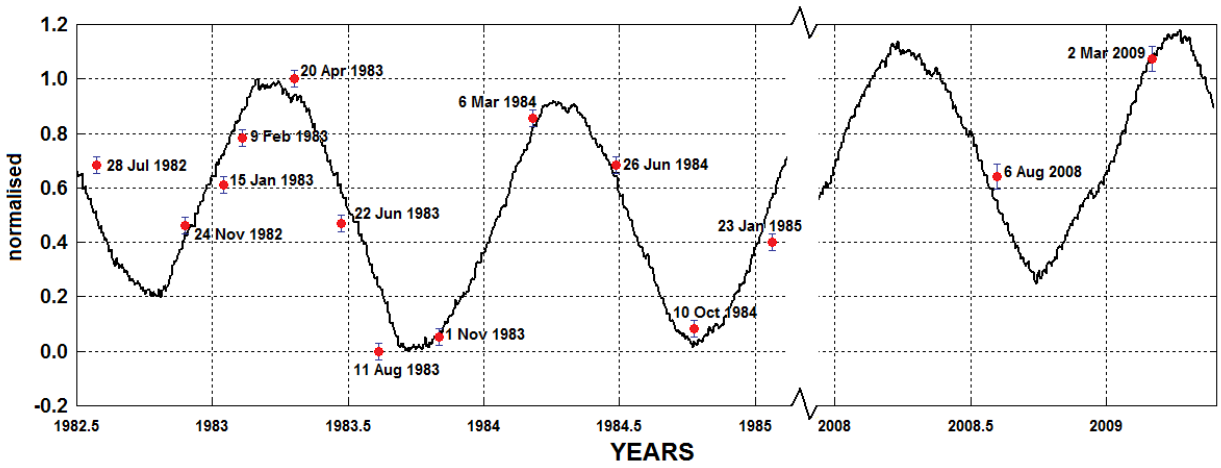

Figure 19. Data from Figure 18 re-plotted with years 1986 to 2007 removed, to show detail.

Had decadal shifts of net evaporation caused irreversible ('ratcheted') responses of salinity, then the net evaporation shifts that have occurred between the 1980s and the late 2000s would have destroyed the earlier relationship, and the fit to recent data would be poor. It is apparent in these results that the mean salinity of northern Spencer Gulf has tracked the 1980s calibration quite closely across a period of nearly three decades, despite the presence of substantial intra- and inter-decadal trends evident in the net evaporation data (Figure 18). From this it is deduced that mean NSG salinity at any particular time is primarily determined by the cumulative effects of net evaporation during the preceding six months, and that the Gulf is not significantly influenced by environmental forcing on longer time scales. This result may be used to determine a calibration of changes in NSG salinity relative to changes of net evaporation, in the next section.

4 Calibration of Salinity Change in Northern Spencer Gulf to Net Evaporation

4.1 Behaviour from 1982 to the present

The results above imply that a change of net evaporation (measured at a South Australian land station) is correlated with a change of mean salinity in northern Spencer Gulf. The relationship can be deduced by carefully comparing the variations of both properties without normalising either. However, some consideration of the effects of filtering a periodic time series is required.

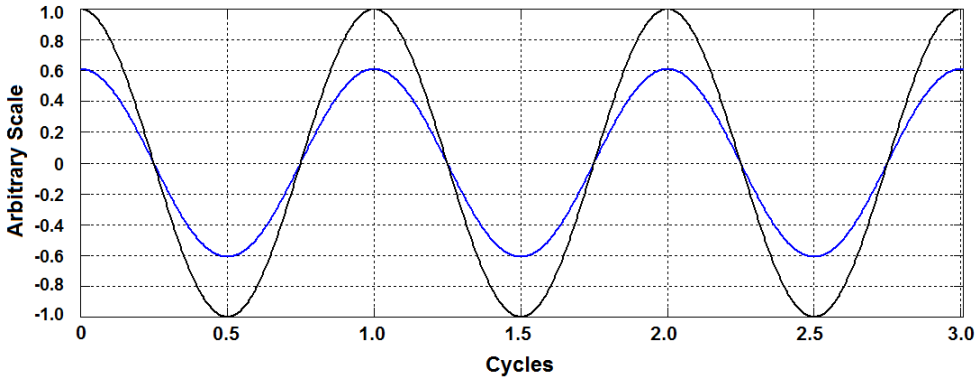

Figure 20. The effects of filtering a periodic time series, as discussed in the text.

Figure 20 shows a periodic time series (in black) with an amplitude of one unit and a notional period of 365 times the interval between individual values, representing an annually varying quantity sampled on a daily basis. The series (in blue) with an amplitude of approximately 0.6 units is the result of applying a (central) filter of 190 samples (or days) in length, showing that the amplitude of the filtered result is substantially smaller than its unfiltered equivalent. The reduction depends on the filter length and its relationship with the period of the series. For an annual period variable, filtered using a 190d filter, the amplitude is reduced to 0.61 of the unfiltered amplitude. A filter length of 192d, produces a series with an amplitude reduced by the factor 0.60.

Figure 21 shows the result of this process applied to net evaporation measurements from Adelaide Airport[7]. Individual points represent daily measured values (with a mean of 2.4 millimetres per day). The 190d filtered result is shown as a solid red line. Increasing the amplitude of the filtered result by dividing by the factor 0.61, also ensuring that the means coincide, produces the result shown as the blue solid line in Figure 20. The 'filtered and adjusted' result represents the smoothed daily variation of net evaporation.

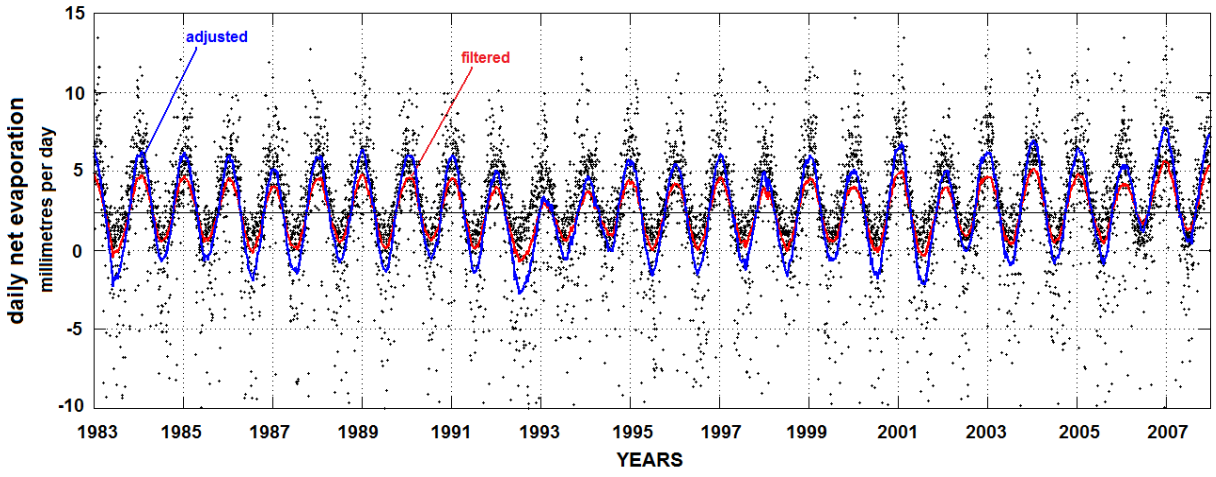

Figure 21. Net Evaporation at Adelaide Airport, with 190d filter applied (red solid line) and the filtered result adjusted to compensate for amplitude reduction due to filtering (blue solid line).

Figure 22 shows the mean salinity of NSG as measured on fourteen occasions between July 1982 and March 2009, with 'filtered and adjusted' values of net evaporation from Price on

[7] Adelaide Airport was chosen for illustration because Price and Spalding data suffer from many missing daily values.

the same days. The least squares regression result (with a correlation coefficient of 0.89) is also plotted on the Figure. The result indicates that a sustained change of one millimetre per day of net evaporation corresponded to a change of mean NSG salinity of 0.230gl^{-1}. For completeness, the regression result fitted to 1980s data alone gave a gradient of 0.228gl^{-1} and a correlation coefficient of 0.87.

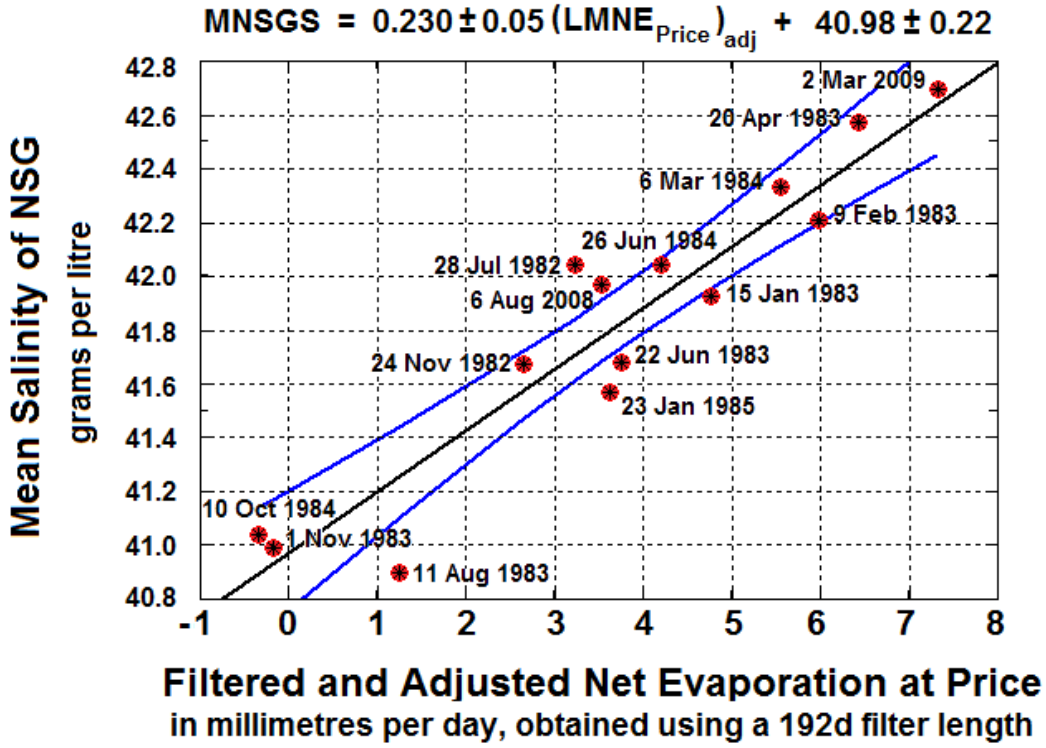

Figure 22. Mean Salinity of NSG against corresponding values of filtered and adjusted net evaporation from Price (using a 192d filter). The least squares regression result is plotted together with 95% confidence intervals.

Based on this relationship, by using net evaporation as a proxy (hindcast) indicator, the historical behaviour of salinity in NSG during the period 1982 to 2009 may be inferred. Figure 23 shows the NSG mean salinity time series inferred from its relationship with net evaporation, together with 3-year and 5-year central running means.

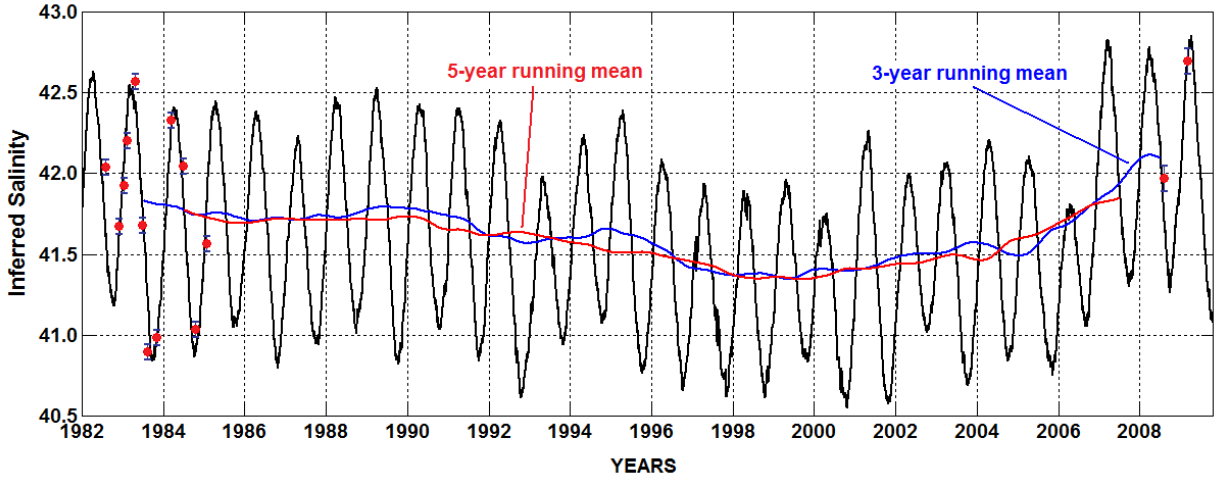

Figure 23. Inferred behaviour of NSG salinity during the past 27 years, with 3-year and 5-year central running means. Discrete observations of mean NSG salinity are also shown together with error bars.

Results inferred from this proxy suggest that, during the period 1982 to 2009, the mean salinity of NSG was 41.56gl^{-1}; the annual mean peak-to-trough variation was 1.38gl^{-1}, with the mean annual peak being 42.25gl^{-1}; the lowest annual average salinity occurred from 1-July-1997 to 30-June-1998 with a value of 41.25gl^{-1}; the highest annual mean salinity occurred in the year 1-July-2007 to 30-June-2008 with a mean of 42.02gl^{-1}; thus the annual mean salinity of NSG rose by 0.77gl^{-1} during the ten year period to 2007/8. The annual salinity maximum was reached, on average, on 12th April, and the annual minimum on 14th October.

5 Natural & Anthropogenic Influences on Northern Spencer Gulf Salinity

5.1 Potential Desalination Impacts

The process of desalination involves the intake of a continuous flow of ambient seawater from a marine zone, the removal of salt from a fraction (typically 40% to 45%) of the flow which is tapped off as freshwater, and discharge of the remaining flow, which carries away the same amount of salt as the original inflow, at an elevated (typically nine-fifths of the original) salinity. Thus, the net effect of desalination is the removal of freshwater, which is also the net effect of evaporation, although the former acts at a point while the latter acts (approximately) uniformly over a large area.

This distinction in the way desalination and evaporation act is of paramount importance when considering potential effects of localised brine discharge. However, the aim here is to assess its effects on a large volume of Spencer Gulf, that is northern Spencer Gulf, over the long-term.

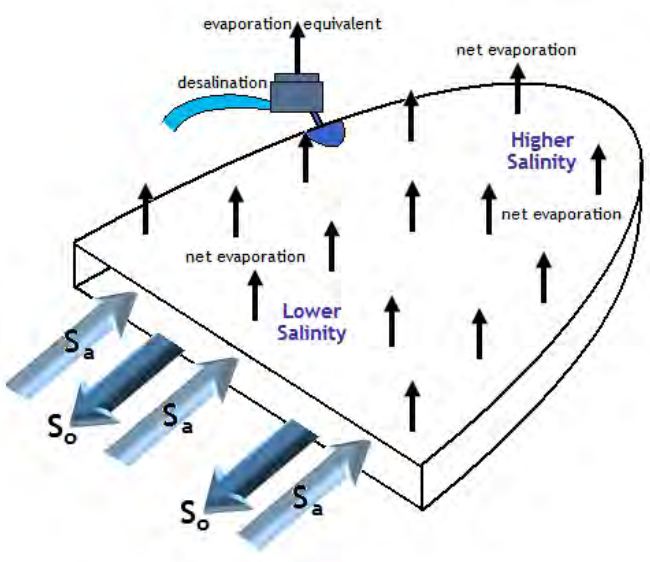

Figure 24. Schematic gulf subject to evaporation and desalination. Note that there is no intention to provide meaningful indication of a 'region of influence' associated with withdrawal from, and discharge of fluids into the Gulf. It is also important to note that the schematic location of the desalination plant puts it entirely within the confines of NSG, which differs from its proposed location at the intersection of NSG and the mid-Gulf. For

this reason, the discussion surrounding this arrangement, in the text, may be considered to over-estimate potential impacts on NSG.

Figure 24 shows a schematic gulf (the same as in Figure 3) with the addition of a desalination plant on its shore. The plant draws in seawater from an undefined zone and discharges brines, as shown here, entirely to northern Spencer Gulf. Thus, freshwater removal by desalination increases the total loss of freshwater from NSG (represented by the vertical arrows in the Figure), which enhances the compensating inflow, S_a, and in turn, raises the mean salinity of NSG (as described earlier).

Regardless of the degree of mixing of desalination return water into NSG, the mean salinity will reflect the gross removal of freshwater (whether localised or not) which drives a compensating landward salt flux, so that desalination acts as a small but equivalent mechanism to evaporation. This report explicitly excludes consideration of any localised effects focusing, instead, on the long-term (measured in months) gross behaviour of NSG, which must respond to desalination in the same way that it responds to evaporation, by elevating mean salinity.

It is also assumed in the following analysis that the desalination plant is sited alongside NSG, and its effects are entirely applied to NSG. This assumption exaggerates potential impacts on NSG because the intake is proposed to be sited very close (of the order of 100m) to Point Lowly (see Figure 2) with the discharge on the Point itself which means, given the generally north-south orientation of tidal flows and the mean effects of the deeper gravitational circulation (discussed in section 6.2), that some of the effects will actually be applied to waters outside NSG.

5.1.1 Quantitative Estimate of Desalination Impact

Referring again to Figure 24, we use the following numerics:

Proposed desalination (or freshwater removal) rate:	251 megalitres day^{-1} $= 2.51 \times 10^8$ litres day^{-1} $= 2.51 \times 10^5$ m^3 day^{-1}
Northern Spencer Gulf:	
Volume	4.4×10^9 m^3
Surface Area	0.52×10^9 m^2
Mean Depth	8.4 m
Whole of Spencer Gulf	
Surface Area	2.2×10^{10} m^2

Assuming that desalination is grossly equivalent to the removal of a freshwater layer from the entire surface area of NSG, the layer thickness is determined as:

(total volume removed by desalination per unit time) / (surface area of NSG)

$$= (2.51 \times 10^5 \text{ m}^3 \text{ day}^{-1}) / (0.52 \times 10^9 \text{ m}^2)$$

$$= 0.00048 \text{ m day}^{-1}$$

$$= 0.48 \times 10^{-3} \text{ m day}^{-1}$$

$$= 1.92 \times 10^{-6} \times \text{DR m day}^{-1}$$

where DR is the desalination rate in megalitres per day. Thus, the evaporation equivalent of desalination is a loss of approximately one half of a millimetre per day from the entire surface of NSG, representing about 15% of the (adjusted) mean daily evaporative loss measured at Spalding and Price between 1982 and 2009. For comparison, the 'best case' alternative scenario in which the freshwater loss is considered to be drawn from the entire surface area of Spencer Gulf implies that desalination effectively removes a surface film of 1.1×10^{-5} m day $^{-1}$, or approximately 0.3% of natural evaporation.

As deduced in section 4.1 (and Figure 22), a freshwater loss of 1×10^{-3} m day^{-1} (in adjusted LMNE at Price) corresponded to a change of MNSGS of 0.23gl^{-1} implying that the gross effects of desalination, if assumed to impact entirely on NSG, are expected to cause an increase of mean NSG salinity of (0.48 x 0.23gl^{-1} or) ~0.11gl^{-1} (or 4.4 x 10-4 x DR gl^{-1}). This represents a rise equivalent to approximately 8% of the mean annual salinity range (1.38gl^{-1}) observed in NSG from 1982 to 2009, implying a rise of annual mean NSG salinity from 41.56gl^{-1} to 41.67gl^{-1}. It also represents a change equivalent to 14% of the 'observed' inter-decadal shift (0.77gl^{-1}) of mean annual NSG salinity between 1997 and 2007, inferred from the net evaporation proxy.

For comparison, using the NSG calibration of salinity with net evaporation, which is expected to over-estimate the salinity response of the whole of Spencer Gulf, the gross impact of desalination on the whole Gulf is inferred to be an increase of mean salinity of ~0.003gl^{-1} (or 1 x 10-5 x DR gl^{-1}).

5.2 Potential Climate Change Impacts

5.2.1 Past Trends in Climate Variables

Suppiah et al (2006, hereafter called S06) report observed trends and modelled predictions of climate change effects on South Australian atmospheric and marine conditions. This report does not question the veracity or validity of these predictions in the context of debate about climate change, but simply accepts the figures in order to deduce potential impacts.

Since the 1950s, South Australia's average air temperature has increased by 0.20°C per decade (the average maximum has increased by 0.21°C and the average minimum by 0.18°C per decade). Sea surface temperatures (SST) have also risen, but by smaller amounts. Specifically between 1900 and 2005, the SST of waters near the mouth of Spencer Gulf has increased by 0.05°C per decade, or at a higher rate of 0.11°C per decade since 1950 (S06).

Over the whole State, rainfall trends were generally weak, showing a small tendency towards wetter conditions in the north of the State, and drier conditions in the southern coastal areas, changing by approximately 5×10^{-3} m decade^{-1} from 1900 to 2005. The period 1950 to 2005 showed a slightly stronger drying trend for coastal regions of up to 10^{-2} m decade^{-1}, although the detail in these observations suggests that the region of NSG may have experienced no significant long-term trend (see Figure 6 of S06). Long-term changes of rainfall were very small, although there were very large inter-annual and inter-decadal variations between 1956 and 2009 from a low of 234.6 millimetres annual rainfall in 2006, up to 730.8 millimetres in 1992, around a mean of 441.7 millimetres (at Adelaide Airport, Bureau of Meteorology online climate statistics[8]).

Evaporation measurements were assessed from US Class A pan evaporation data, which is acknowledged to be prone to significant errors (S06) at three sites, Woomera, Ceduna and

8 http://www.bom.gov.au/jsp/ncc/cdio/weatherData/av?p_nccObsCode=139&p_display_type=dataFile&p_startYear=&p_stn_num=023034

Mount Gambier. Only Woomera showed a statistically significant trend, rising by 11.5×10^{-3} m year^{-1}, each year around a mean of 3.21 m year^{-1}.

5.2.2 Projected 2030 and 2070 Air Temperatures

S06 went on to assess the results of 25 climate models from many different international sources. These models show substantial inconsistencies in their projections of change which, when combined with the Intergovernmental Panel on Climate Change alternative scenarios, lead to predictions of change that fall into broad ranges. With regard to air temperature, South Australia is assessed in three regions: less than 200km from the coast (which we refer to as the 'coastal band'); 200 to 600 km from the coast; and greater than 600km from the coast. We will assume that Spencer Gulf belongs to the coastal band, as continental conditions may overwhelm the small maritime contribution of NSG in the second band. By 2030, air temperature within the coastal band is projected to rise by 0.2°C to 1.6°C, and 2070 projections indicate a rise of 0.5°C to 4.7°C.

S06 also provided projections for the 'National Resource Management' (NRM) regions. The two NRM regions that most closely straddle NSG are those of the 'Northern and Yorke Region' and 'Eyre Peninsula'. Summaries are provided for these regions and are largely consistent between the two. By 2030 air temperature is expected to rise by 0.4°C to 1.2°C, and by 2070 this is projected to be 1.0°C to 3.8°C, so the NRM forecasts are more conservative than those of the coastal band.

5.2.3 Projected 2030 and 2070 Precipitation

Developing forecasts for rainfall is said (S06) to be more complex and less consistent than for temperatures. Using the 30-year annual average rainfall centred on 1990 as the baseline, projections for the coastal band show a change of -15% to 0% by 2030, and -45% to 0% by 2070. Projections for the NRM regions indicate changes of -10% to 0% by 2030, and -30% to -1% by 2070 which are, again, more conservative than those of the coastal band.

5.2.4 Projected 2030 and 2070 Evaporation

S06 did not report evaporation trends, primarily because direct measurement of evaporation is difficult, and evaporation is usually assessed as the residual term in heat budget calculations.

5.2.5 Estimating 2030 and 2070 Climate Change Impacts on the Salinity of Northern Spencer Gulf

In order to deduce climate change effects on NSG salinity, it is necessary to translate their effects into an overall assessment of the change to net evaporation. Estimating evaporation as the residual term in a heat budget calculation will not suffice here because such estimates would inherit the uncertainties present in all other terms.

Two alternative methods to assess evaporation are offered below. Firstly, as noted in the discussion of Figure 10 and section 2.1, evaporation and precipitation appear to be negatively correlated and thus, projections of changing rainfall may be used to deduce evaporation projections. Alternatively, projected changes of air and sea temperature (S06) allow evaporation to be estimated using bulk aerodynamic formulae. Both methods will be used to estimate evaporation in 2030 and 2070 which, combined with the S06 projections of precipitation, yield estimates of net evaporation from which changes to NSG salinity are deduced.

5.2.5.1 Estimating Impacts from Projections of Precipitation

The 3-year running means of evaporation and precipitation at Adelaide Airport (shown in Figure 10) imply a relationship between evaporation and precipitation trends which might be deduced through simple regression. Such a procedure, using annual means, shows that the two parameters are correlated according to:

$$(\text{Evaporation})_{365\text{d mean}} = -0.75 \times (\text{Precipitation})_{365\text{d mean}} + 4.6$$

where both evaporation and precipitation are measured in millimetres per day. This result supports translation of the climate projections of precipitation into estimates of the corresponding evaporation trends.

2030: Suppiah et al (2006) projected precipitation changes within the coastal band for 2030 and 2070 from the 30-year baseline centred on 1990, indicating that a reduction of between 0% and 15% is anticipated in 2030 (a more extreme worst case than was obtained by considering the two NRM regions).

Since Adelaide Airport shows a useful precipitation-evaporation correlation, and it belongs within the coastal band, the result is used as follows. For the 30-year period centred on 1990, the annual average precipitation at Adelaide Airport was measured to be 448 x 10^{-3} m $year^{-1}$ (Bureau of Meteorology[9]).

The 2030 annual average rainfall is consequently projected (S06) to lie within the range 381 x 10^{-3} m $year^{-1}$ to 448 x 10^{-3} m $year^{-1}$. From the regression relationship above, the 2030 annual evaporation is therefore inferred to lie between 1.38 m $year^{-1}$ and 1.33 m $year^{-1}$. Thus, the worst case net evaporation (evaporation minus precipitation) is inferred to be 1.00 m $year^{-1}$, representing an increase of 0.12 m $year^{-1}$ or 0.32 x 10^{-3} m day^{-1} over 1990-centred average conditions

2070: S06 projected a reduction of precipitation in the coastal band of between 0% and 45% by 2070, thus precipitation at Adelaide Airport is expected to lie within the range 246 x 10^{-3} m $year^{-1}$ and 448 x 10^{-3} m $year^{-1}$ in 2070 (noting that projections for the NRM regions were less extreme than this).

Evaporation is consequently projected to lie between 1.48 m $year^{-1}$ and 1.33 m $year^{-1}$, leading to a worst case increase of net evaporation in 2070 of 0.35 m $year^{-1}$, or 0.97 x 10^{-3} m day^{-1} over 1990-centred values.

5.2.5.2 Estimating Net Evaporation Changes from Projections of Air Temperature and Precipitation

Estimates of evaporation may be obtained using bulk aerodynamic formula (see, for example, Brutsaert, 1982; and Holloway, 1980), as follows. The bulk aerodynamic formula for the latent heat flux (He) associated with evaporation is given as:

$$H_e = \rho_a \, L \, C_E \, u_{10} \, (q_0 - q_{10})$$

where ρ_a is the density of air, L is the latent heat of vapourisation of water, C_E is the bulk transfer coefficient for moisture (~0.0019), u_{10} is the wind speed at the standard meteorological height of ten metres, and q is the specific humidity at the surface (suffix of zero) and at ten metres (suffix of 10).

The specific humidity is given by:

$$q = (0.622\ e) / (P - 0.378\ e) \approx 0.622\ e / P$$

[9] http://www.bom.gov.au/climate/averages/tables/cw_023034.shtml

where P is atmospheric pressure, and e is the vapour pressure, which is temperature-dependent according to the following polynomial:

$$e_s(T) = a_0 + a_1.T + a_2.T^2 + a_3.T^3 + a_4.T^4 + a_5.T^5$$

in which a_0 = 6.11, a_1 = 4.44 x 10^{-1} , a_2 = 1.42 x 10^{-2}, a_3 = 2.71 x 10^{-4}, a_4 = 2.74 x 10^{-6} and a_5 = 2.73 x 10^{-8}.

Evaporation is driven by the gradient of specific humidity between the water surface and 10m height, which is given by:

$$q_0 - q_{10} \approx [e(T_0) - e(T_{10})] / (1.61\ P) = [e_s(T_0) - R.e_s(T_{10})] / (1.61\ P)$$

where the vapour pressure at 10m height is equal to the saturated vapour pressure times the relative humidity (R) at 10m, leading to estimation of evaporation changes according to projected changes in air and sea-surface temperatures.

2030: Projections of mean atmospheric temperature rise in the coastal band for the 2030 timeframe (S06) were between 0.2°C and 1.6°C. Based on historic data for the last half century S06 also noted that sea-surface temperature (SST) near the mouth of Spencer Gulf had risen at approximately half the rate of air temperature. It might be argued that SST within Spencer Gulf, particularly NSG, should more closely match the full magnitude of the rise in air temperature. However, using different rates produces a larger atmospheric vapour pressure gradient and hence greater evaporation, representing a worst case scenario. On this basis, it is inferred that SST in NSG in 2030 will have risen by 0.1°C to 0.8°C.

Mean summertime daily-maximum air temperatures at Port Augusta Power Station (the top of NSG) between 1962 and 1997 were approximately 31°C (Bureau of Meteorology), while SSTs in NSG were measured (NL86) at approximately 24°C. Daily peak summertime latent heat fluxes using these temperatures (and assuming a relative humidity of 75%, the approximate average summertime value coincident with peak daily air temperatures, recorded at Yarraville Shoal, 33° 17'S 137° 35.6'E, approximately 35km south-south-west of Point Lowly, Nunes-Vaz data) gives a peak evaporation rate of 2.7 x 10^{-8} ms^{-1}. Assuming that, in 2030, mean daily-maximum air temperatures will have risen to 32.6°C, with NSG SSTs at 24.8°C leads to a peak evaporation rate of 4.0 x 10^{-8} ms^{-1}, representing a 45% increase in peak evaporation.

Making the two further assumptions that daily evaporation is sinusoidal between zero and the peak daily value, and that the annual evaporation is also sinusoidal, with an annual mean of approximately half the summertime peak (both of which are approximately true from observations), implies that the 2030 estimate of evaporation is approximately 11% larger than 1990 values, reaching 1.47 m $year^{-1}$. Combining this with the projected change of precipitation implies that mean annual net evaporation in 2030 will reach 1.09 m $year^{-1}$, an increase of 0.21 m $year^{-1}$.

2070: A similar procedure, assuming that air temperature rises to 35.7°C and the sea temperature rises to 26.3°C implies that annual evaporation increases to 1.83 m $year^{-1}$ and mean annual net evaporation in 2070 will reach 1.59 m $year^{-1}$, an increase of 0.71 m $year^{-1}$.

5.2.5.3 *Implied Effects on Northern Spencer Gulf Salinity*

With these estimated changes, it is now possible to provide inferred impacts on NSG salinity, based on the result of section 4.1.

2030: Projections of precipitation changes for 2030 (S06) indicate an increase in net evaporation of 0.32 x 10^{-3} m day^{-1}, which implies an increase in NSG salinity of 0.07gl^{-1}.

Air and sea temperature projections, combined with projections of precipitation changes, indicate an increase in net evaporation of 0.21 x 10^{-3} m day^{-1}, which implies an increase in NSG salinity of 0.05gl^{-1}.

2070: Projections of precipitation changes for 2070 (S06) indicate an increase in net evaporation of 0.97 x 10^{-3} m day^{-1}, which implies an increase in NSG salinity of 0.22gl^{-1}.

Air and sea temperature projections, combined with projections of precipitation changes for 2070, indicate an increase in net evaporation of 0.71 x 10^{-3} m day^{-1}, which implies an increase in NSG salinity of 0.16gl^{-1}.

These results are collected, together with the estimated impacts of desalination and the observed natural variation of salinity between 1982 and 2009, in Table 2.

Influence	Based on	Change of Net Evaporation (x 10^{-3} m day^{-1})	Change of NSG mean salinity g l^{-1}	Inferred Mean Salinity g l^{-1}	Impacts, Relative to Natural Variation
Annual Variation	Mean 1982 to 2009	6.0	1.38	41.56	100%
Desalination	180 x 10^{6} litres day^{-1}	< 0.35	< 0.11	41.67	8.0%
Climate Change 2030	Precipitation (P)	< 0.32	< 0.07	41.63	5.3%
	Temperatures and P	< 0.21	< 0.05	41.61	3.5%
Climate Change 2070	Precipitation	< 0.97	< 0.22	41.78	16%
	Temperatures and P	< 0.71	< 0.16	41.72	12%

Table 2. The observed, calculated and predicted changes of net evaporation from northern Spencer Gulf, and their implied effects on mean salinity.

5.3 Summary of Anthropogenic Influences on Mean NSG Salinities

This assessment has produced estimates of the change of mean salinity in northern Spencer Gulf associated with desalination and climate change predictions (for 2030 and 2070), summarised in Figure 25 and the series of graphics shown in Figure 26. Note that climate change projections in S06 were referenced to mean conditions centred on 1990 (from 1975 to 2004). Evaporation data from Price were not available until 1977, but the 1977 to 2004 mean was almost identical to the mean calculated for 1982 to 2009, which is why the latter interval is used to represent mean behaviour of NSG centred on 1990.

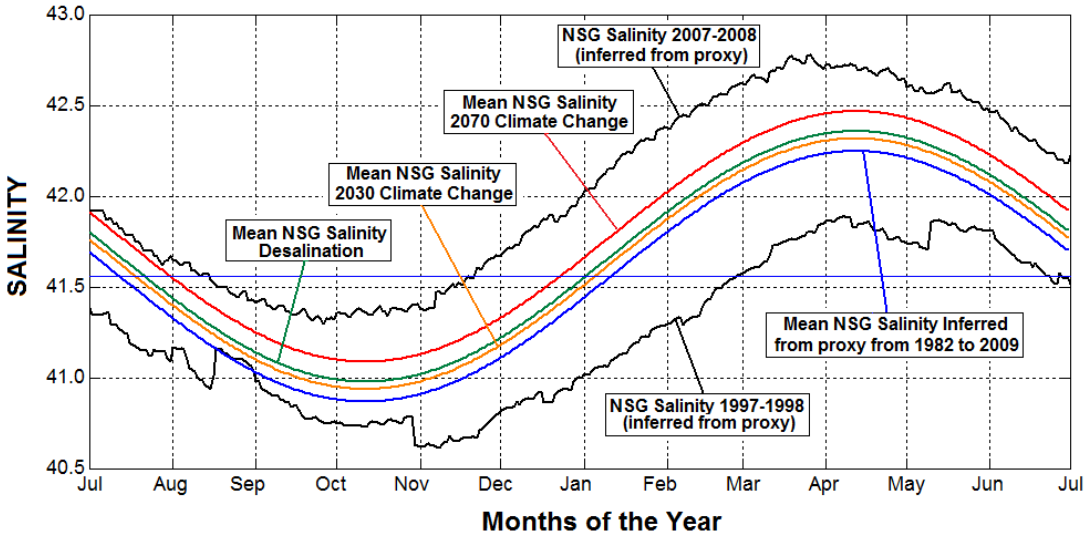

Figure 25. Mean annual salinity variation in NSG inferred from the Price LMNE proxy (blue) together with inferred salinity cycles that include the effects of: desalination (green); climate change in 2030 (orange); and climate change in 2070 (red). The inferred NSG salinities during 1997-98 and 2007-08 (in black) are included to indicate the extent of inter-annual variability, noting that these traces include the effects of large precipitation variability and irregular digitisation associated with the collection of meteorological data.

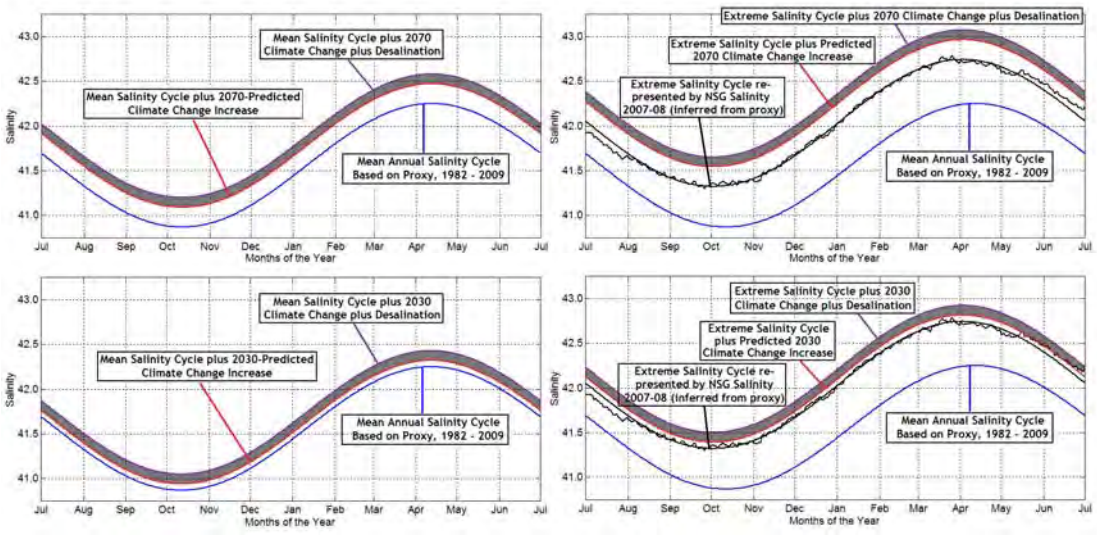

Figure 26. Four panels showing comparative estimates of both climate change and desalination impacts on NSG salinity. The upper-left panel compares 2070 climate change alone, and combined with desalination, on the mean annual salinity cycle inferred between 1982 and 2009. The upper-right panel shows these perturbations as additions to the most extreme annual salinity cycle inferred between 1982 and 2009. The lower-left and lower-right panels are equivalent to the upper panels, where predictions of the impact of 2030 climate change have been substituted for those of 2070.

The strong blue lines in Figure 26 are all equivalent and show the annual mean salinity cycle inferred from net evaporation between 1982 and 2009 (mean 41.56gl^{-1}, amplitude 0.69gl^{-1}).

Irregular (black) traces (and their smoothed interpretation) show the inferred cycle for 2007-08 (mean 42.02gl^{-1}) which was the highest mean salinity cycle inferred from the proxy between 1982 and 2009. The impacts of climate change (red), and then in combination with desalination (the additional grey band) are represented as perturbations to the mean salinity (left panels) and to the highest extreme salinity (right panels) for both 2070 (upper) and 2030 (lower) climate change predictions.

With respect to worst case scenarios, combining the impacts of desalination and climate change with the mean of the highest annual cycle of salinity inferred from the past 27 years (in 2007-08), the mean salinity of NSG is expected to rise to 42.20gl^{-1} in 2030 (lower-right panel of Fig 25), and 42.35gl^{-1} in 2070 (upper-right panel). These results represent increases of 46% and 57%, respectively, of the mean annual salinity variation (of 1.38gl^{-1}) inferred between 1982 and 2009. The peak salinities for the extreme salinity cycles shown in Figure 26 would be 42.92gl^{-1} and 43.07gl^{-1}, for 2030 and 2070 respectively, compared with the annual mean peak of 42.25gl^{-1} (as shown by the blue line in Figure 26).

At this point, the first two driving questions have been resolved, that is:

1. how Spencer Gulf responds to influences that disturb its salinity, and how long it takes to 'recover' following a disturbance, and
2. the degree or extent to which salinity is expected to change in response to a disturbance.

The next section addresses the last of the three questions, namely:

3. whether anticipated perturbations associated with desalination and climate change will be large enough to shift the Gulf's salinity, irreversibly, to a new equilibrium state.

6 Equilibrium Dynamics of Oceanographic Salt Exchange in North Spencer Gulf

To answer the third question above requires examination of the nature of oceanographic salt exchange processes operating in Spencer Gulf. As briefly discussed in section 1.1, there are two processes that contribute to the transport of salt down the Gulf's natural salinity gradient, namely gravitational circulation, and turbulent diffusion and dispersion. Both contribute to the maintenance of a long-term equilibrium and each dominates the other in different (wind, tide and current) conditions, locations and times (for example, seasons).

However, the assessment may be made relatively straightforward by examining each mechanism in turn, to ask whether there might be a natural limitation on the exchange that each can achieve individually.

6.1 Horizontal Gravitational Circulation

NV90 used a simple two-dimensional (flat) representation of Upper Spencer Gulf (see Figure 27) characterised by two contributions to flow, namely: a net inflow, at speed u_E, re-supplying the fluid lost by net evaporation (which was also shown schematically in Figure 3); and a horizontal circulation at speed u_C, carrying lower salinity fluid (s_i) northward on the western side, and higher salinity fluid (s_o) southward on the eastern side, to account for the observed two-dimensional orientation of isohalines. In this arrangement, NV90 showed (their equation 3) that the circulation speed is given by:

$$u_c = \frac{2(E - P).A}{bh} . \frac{s_i}{(s_o - s_i)} \qquad (1)$$

where $(E - P)$ is the net evaporation from surface area A, b is the horizontal width and h is the depth of the southern section through which the flows occur. Assuming that all quantities are fixed, including the salinity of the inflow (s_i), the salinity of the outflow will increase as the speed of the circulation decreases. Intuitively, this means that a more sluggish circulation is more affected by evaporation causing the outflow salinity to be correspondingly higher.

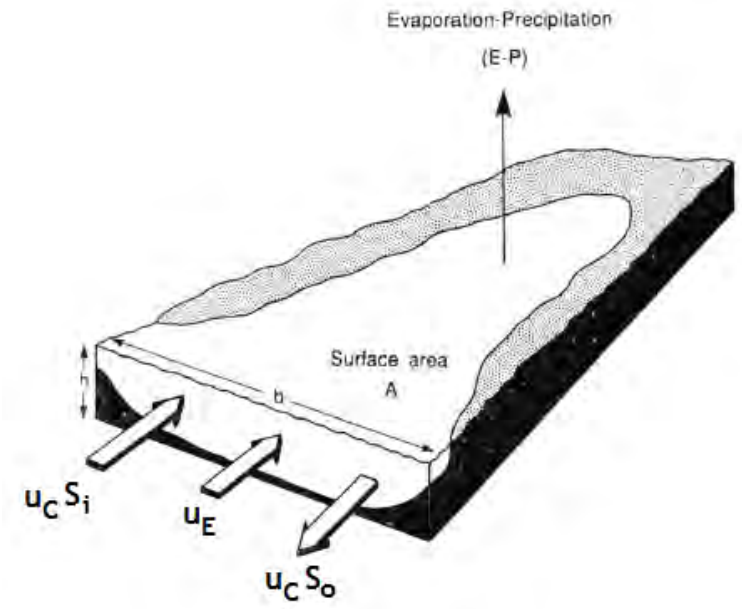

Figure 27. Schematic Two-Dimensional Salt Exchanges in Spencer Gulf (reproduced from Nunes Vaz et al, 1990)

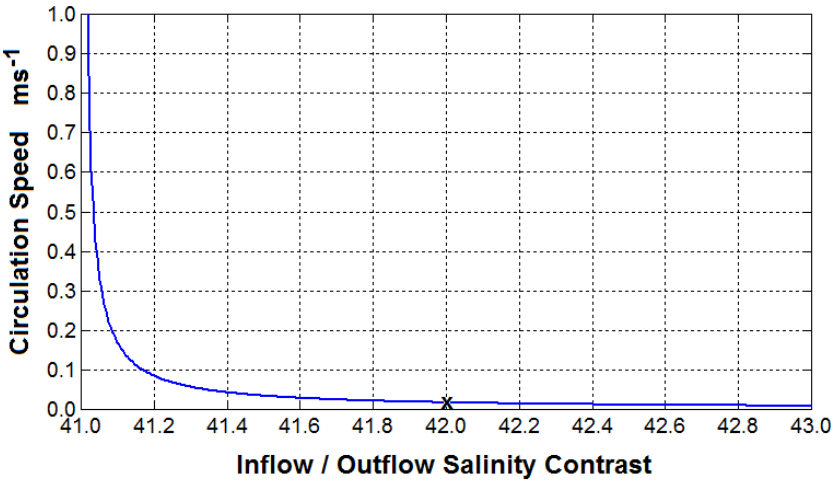

Figure 28. The relationship between circulation speed and inflow-outflow salinity contrast defined by equation (1)

Taking the southern boundary to be at 33°S (the southern limit of NSG as defined here), and using the data of NV90 (i.e., $(E - P) \approx 4.4 \times 10^{-8}\ ms^{-1}$, $A \sim 6 \times 10^{8}\ m^2$, $b \sim 1.6 \times 10^{4}\ m$, $s_i \sim 41 gl^{-1}$) with $h \sim 8.4m$ Figure 28 shows the relationship between circulation speed and the inflow-outflow salinity contrast. Assuming, as in NV90, that the outflow salinity $s_o \sim 42 gl^{-1}$ implies that u_C is approximately 0.02 ms^{-1}. Thus, a rather modest net circulation is required to account for the flushing of excess salt from NSG produced by net evaporation.

As these flows are horizontally distinct, there is only one conceptual limitation on the net flux of salt they are able to achieve, which is set by the hydraulics of the channel in which the flows take place. The hydraulic limit is represented by a Froude number, Fr, (see any hydraulics text):

$$Fr = \frac{u}{\sqrt{gh}} \tag{2}$$

where g is the acceleration of gravity, u is a velocity and h is a depth, which expresses the notion that the gravitational potential energy of the system (represented by the denominator) can sustain a flow at the control section (which we take to be 33°S) to produce a Froude number no greater than one. This limit is achieved where $u = \sqrt{gh}$ implying an upper limit on the circulation speed of approximately 8 ms^{-1}. Clearly this does not constitute a significant constraint on horizontally distinct exchange flows.

However, there is no dynamic mechanism able to sustain the complete lateral separation between inflow and outflow in the presence of gravity. Ignoring the Earth's rotation, the flows would instead be vertically differentiated (with a low density inflow above a high density outflow), which is considered next.

6.2 Vertical Gravitational Circulation

Spatially differentiated exchange flows influenced by gravity in a non-rotating frame of reference are vertically juxtaposed, separated by a horizontal interface with inflow and outflow layers each occupying approximately half the depth. The two layers (with densities ρ_i and ρ_o, where the subscripts represent the less dense inflow, *i*, and more dense outflow, *o*) remain stable in the presence of shear across the interface until the gradient Richardson number, R_i, decreases to approximately 0.25 (Turner, 1973). The gradient Richardson number is given by:

$$R_i = \frac{g'h}{(u_o - u_i)^2} \tag{3}$$

in which h is the vertical scale of the interface, and g' is the reduced gravity (given by $g.(\rho_o - \rho_i)/\rho_o$ which assumes that the Boussinesq approximation is valid, that is, density differences are small). Large Richardson numbers represent stable conditions. As the Richardson number approaches 0.25, the energy imparted by the shear across the interface becomes sufficient to overcome the stability of the stratification, and the interface typically forms large rolling (Kelvin-Helmholtz) billows that rapidly achieve vertical mixing of scalar properties (such as salinity or density) and momentum.

Thus, an organised vertically differentiated inflow/outflow is able to support the net exchange of salt until either the density contrast falls, or the shear increases such that R_i approaches 0.25. When such an interface becomes unstable, both the density contrast and the shear are suddenly reduced in a catastrophic breakdown of the exchange flow arrangement. This is the limit that must be understood because it represents a potential limit to the maintenance of an equilibrium between the processes that generate an excess of salt in NSG, and those that remove it.

An alternative stability criterion is represented by the internal or densimetric Froude number, Fr_i, given by

$$Fr_i = \frac{u}{\sqrt{g'h}} \tag{4}$$

noting that reduced gravity replaces normal gravity in equation (1). While the use of a Richardson number stability criterion would be preferred, it is not possible to estimate pre- and post-mixing interface thicknesses. The internal Froude number uses a characteristic vertical scale of, *h*, the layer depth rather than the interface thickness, and is therefore more easily applied. A stratified shear flow loses stability as the internal Froude number increases and approaches unity.

Re-interpreting the horizontal net circulation discussed in section 6.1 as a vertically-differentiated exchange flow with each layer occupying half the depth, equation (1) describes the relationship between the vertical shear (twice the circulation velocity) and the vertical salinity contrast. Thus, for given environmental conditions, equation (4) can be used to quantify the internal Froude number.

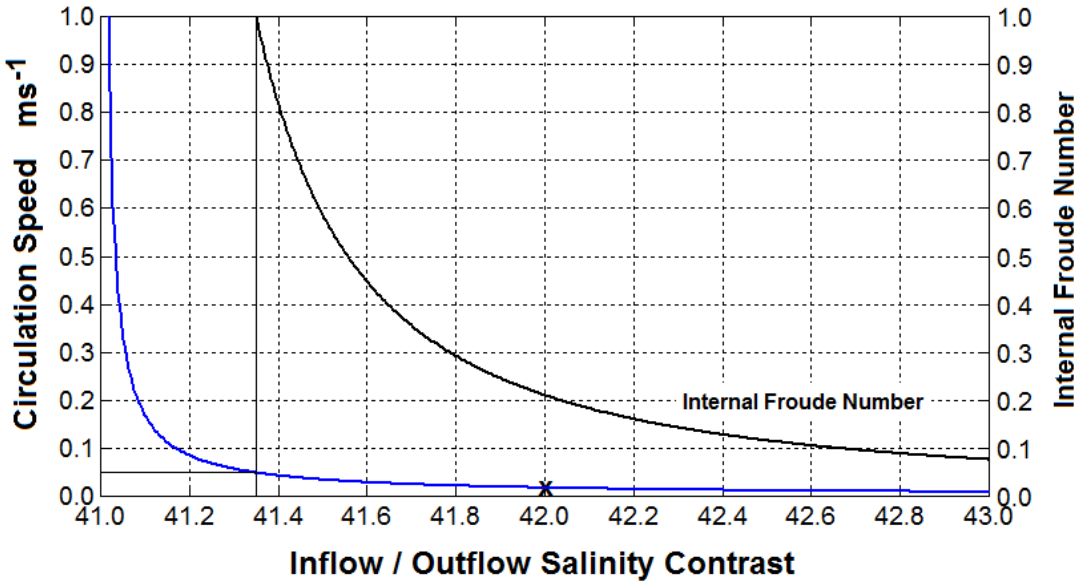

Figure 29. Theoretical speed of the southward circulation component, as a function of its salinity, required to maintain the long-term salt balance of NSG (assuming that the salinity of the northward component is 41.0gl^{-1}). The internal Froude number of the stratified exchange flow is also shown.

Assuming that the balance expressed by equation (1) applies to a vertically separated exchange circulation, and that the inflow salinity (s_i) remains at 41.0gl^{-1} (anchored by conditions further south) the relationship between the outflow salinity and the circulation speed (Figure 28) implies that as the salinity contrast between inflow and outflow decreases, both the circulation speed and, through equation (4), the internal Froude number, increase. Figure 29 indicates that internally critical flow ($\text{Fr}_\text{i} \sim 1$) is reached when the outflow salinity falls to 41.35gl^{-1} which implies that, if the exchange circulation were entirely vertically-separated then the discharge of excess salt from NSG could not be maintained if the average salinity contrast between inflow and outflow fell below 0.35gl^{-1}. Limited data obtained from NSG do not have adequate spatial and temporal resolution to indicate whether in fact the section maintains stratification to this degree, but this appears to be quite a stringent condition with regard to the discharge of excess salt.

Continuing this line of thought, assuming that this cross-section remains a control section for the internal hydraulics as additional stresses associated with desalination and climate change are applied, manipulation of equations (1) and (4) implies that the vertical salinity stratification must increase with $(E-P)^{2/3}$. Thus, if net evaporation increases by 10%, the salinity stratification at 33°S must rise by 6.5% implying that the deep outflow salinity must

rise from 41.35gl^{-1} to 41.37gl^{-1}, a very modest adjustment, to maintain the equilibrium exchange.

6.3 Gravitational Circulation Including Earth's Rotation

In fact neither the horizontally-differentiated nor vertically-differentiated flows are physically realistic solutions because the Earth's rotational (Coriolis) effects are important at this scale. The effect of rotation is to tilt the interface away from the horizontal, more so as the rotational effects increase, so that the horizontal differentiation between the flows increases. Ou (1984) showed that the distance between the interface intersections with the surface and the sea bed is approximately twice the internal Rossby radius of deformation, Ro_i, given by:

$$Ro_i = \frac{\sqrt{g'h}}{f} \qquad (5)$$

where f is the Coriolis parameter $2.\Omega.\sin\phi$, in which Ω is the rotation rate of the Earth (7.29 x 10^{-5} rad s^{-1}) and ϕ is the latitude. Thus as f increases the Rossby radius decreases and the interface becomes more vertical.

The stratification range shown in Figure 29 implies an internal Rossby radius of between a few hundred metres and approximately three kilometres, compared to the width of NSG at 33°S which is more than 7 kilometres. Thus, the interface between inflow and outflow (see Figure 30) is inferred to be more vertical than horizontal implying that the horizontally separated exchange circulation (discussed in section 6.1) is a better model than the vertically separated case (discussed in section 6.2). Consequently, the exchange circulation is unlikely to be limited to any significant extent by an interfacial stability criterion.

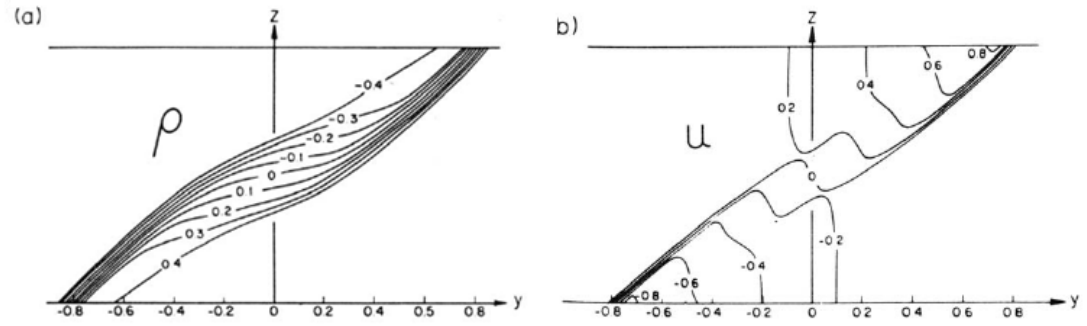

Figure 30. (a) Smoothed version of the steady-state density field after geostrophic adjustment from an initial vertically-uniform non-linear horizontal gradient. The horizontal scale, y, is measured in units of the internal Rossby radius of deformation. (b) The corresponding geostrophic velocity field perpendicular to the plane of the diagram – in the case of Spencer Gulf, a negative velocity should be interpreted as a southward outflow. Reproduced from Ou (1984).

6.4 The Role of Temperature in Driving Gravitational Circulation

Given that the effects of climate change are expected to include elevation of Gulf temperatures, it is important to assess the role of temperature in the Gulf's gravitational exchange processes, and whether higher temperatures may have an adverse effect on the exchange mechanisms. The gravitational exchange is driven by along-Gulf density differences, and both temperature and salinity affect density, although by differing amounts. Temperature affects density through the thermal expansion coefficient, which is

approximately 1.7 x 10^{-4} per °C, that is, the density decreases by approximately 0.017% for each degree of temperature rise. Similarly, the haline contraction coefficient is approximately 7.8 x 10^{-4} per gl^{-1} of salinity change, or density increases by 0.078% for each gl^{-1} of salinity increase. Thus the effect of salinity (in gl^{-1}) on density is approximately 4.6 times that of temperature (in °C)[10].

NL86 reported temperature as well as salinity from each of the twelve 1980s Gulf surveys. They showed (NL86, Figure 4) that the temperature difference from the head of the Gulf to 33°S (i.e., along NSG) reaches a maximum in January of approximately 2°C. Equivalently, the maximum salinity difference reaches approximately $7gl^{-1}$, in autumn. These temperature and salinity gradients (both with higher values at the head) act on density in the opposite sense, such that the temperature contribution reduces the contribution of salinity to the density gradient, by approximately 6%. At other times of the year, when the temperatures are relatively low at the head, the temperature gradient reinforces the salinity gradient and strengthens the density gradient.

Thus, climate change must produce a rather large difference between the temperatures at Port Augusta and those at Point Lowly if the temperature gradient is to play a significant role in reducing the density-induced forcing of gravitational exchange.

6.5 Turbulent Diffusion

The alternative to an organised gravitational exchange circulation involves turbulent diffusion and dispersion (Fischer et al, 1979), represented (see NL86) by:

$$\frac{\partial s}{\partial t} = \frac{(E-P)}{h}.\, s + K_x \frac{\partial^2 s}{\partial x^2} \qquad (5)$$

where variables retain their former meanings, x is an along-Gulf coordinate with its origin at the head, and K_x is the along-Gulf eddy diffusion coefficient associated with boundary-induced and internal sources of turbulence. Using the observed annual mean salinity gradient, NL86 (see their Figure 7) deduced that the diffusion coefficient required to maintain a southward diffusive salt flux equal to the northward flux associated with evaporation, is characterised by values of ~10 m^2s^{-1} near the head, increasing to ~100 m^2s^{-1} at the southern limit of NSG (at 33°S).

Assuming that NSG maintains a steady (repeatable annual mean) salinity gradient along its axis removes the time-dependency, and leads to:

$$(E - P) = - h K_x . \frac{1}{s} \frac{\partial^2 s}{\partial x^2} \qquad (6)$$

which shows that a change of net evaporation requires an adjustment of the curvature of the along-gulf salinity gradient, assuming that levels of turbulence (generated by winds, for example) do not also change.

Using a simple inverse logarithmic representation of the along-gulf salinity variation indicates that a 10% increase in net evaporation requires an increase of NSG mean salinity from $41.56gl^{-1}$ to $41.74gl^{-1}$ to maintain the equilibrium southward diffusive flux of salt. Thus, again, if this were the only mechanism responsible for maintaining the salt balance of NSG, then it is inferred that relatively modest adjustment of the along-gulf salinity gradient would be sufficient to respond to projected environmental changes brought about by desalination or climate change.

[10] The thermal expansion and haline contraction coefficients are temperature, salinity and pressure dependent.

In addressing the third driving question, this assessment of mechanisms that contribute to the maintenance of the Gulf's salt balance has shown that none is sufficiently close to a stability limit as to imply that additional environmental stresses may tip the balance towards a breakdown of the equilibrium between salt inflow and outflow. Each mechanism responds to an increase of net evaporation by a positive adjustment of the along-Gulf salinity gradient, in different measure according to the mechanism in question. However, each is able to maintain the equilibrium dynamics with only moderate changes to the mean salinity of northern Spencer Gulf.

6.6 The Assumption of a Steady Seaward Salt Flux

The suggestion that oceanographic processes removing salt from Spencer Gulf are constant all year round seems (at first sight) to be at odds with earlier publications of this author on the behaviour of the Gulf, and its tendency to generate discrete seasonal (and springs-neaps) salt discharge events, most notably in autumn.

However, observed periodic discharges, and their theoretical foundation (as developed in NL86, Nunes & Lennon, 1987, and NV90), are in fact strongly depth-dependent. While Spencer Gulf is characterized by substantial horizontal salinity (and density) gradients, observations indicate that it is usually reasonably well-mixed in the vertical. This indicates that turbulence generated at the surface by winds, and internally and at the sea-bed by (for example, tidal) currents is normally adequate to overcome the stratification which is continually created by gravitational circulation.

The energy required to mix a stratified water column scales with the depth, that is, once stratified it takes more energy to mix a deep, than a shallow water column with the same surface-to-bottom density contrast. This means that, once established, it is harder to mix out a dense bottom current in a deep part of Spencer Gulf (in the south) compared with one in shallower regions (in the north). For this reason, once established, dense bottom outflows are likely to be more persistent as they extend into deeper waters.

The unusual tidal regime in South Australia (the equality of lunar and solar semi-diurnal tidal influences which are responsible for the 'dodge tide') means that tidal currents fall to very low levels on a fortnightly basis. When such conditions are coincident with light winds, boundary-generated turbulence is greatly curtailed and the ubiquitous influence of gravitational circulation is able to generate stratification. Nunes & Lennon (1987) show that the rate at which stratification develops when turbulence decays, scales as the inverse-square of the depth, which means that stratification develops more rapidly in shallower waters than in deep.

Thus differing characters of behaviour are expected between the northern and southern parts of Spencer Gulf. In the shallower north, stratification may develop quite quickly in response to reduced turbulence, and may even develop to some extent, during the turn of the tide, provided winds are also light. However, relatively little energy is required to mix out any stratification once it appears, so the character of NSG is expected to show frequent and rapid onset of minor stratification that is also destroyed quite quickly. Contrastingly, while it is takes longer, and therefore requires sustained periods of low turbulence to establish significant stratification in the deeper, southern parts of Spencer Gulf, once it is established it is much more persistent and resistant to turbulent mixing. The southern Gulf is therefore expected to show much fewer, but longer-lasting (e.g., seasonal) stratified discharge events.

The frequent, short-lived stratified exchange circulation events seen in northern Spencer Gulf are therefore considered to be a reasonable approximation to steady discharge, for the purposes of this report.

7 Summary and Discussion

This report has examined issues surrounding the long-term balance and distribution of salt in Spencer Gulf in order to understand and quantify the potential effects of desalination and climate change. The analysis focused on three primary questions:

- how Spencer Gulf responds to influences that disturb its salinity, and how long it takes to 'recover' following such a disturbance,
- the degree or extent to which salinity is expected to change in response to a disturbance, and
- whether anticipated perturbations associated with desalination and climate change will be large enough to shift the Gulf's salinity, irreversibly, to a new equilibrium state.

Spencer Gulf is an inverse estuary characterised by salinities that reach ~48gl^{-1} at the head in summer. The origin of the Gulf's elevated salinities is the result of freshwater loss by evaporation which is replaced by a northward flow of seawater. Focusing on 'northern Spencer Gulf' (NSG), or the region north of 33°S, the southward flux of salt which is required to maintain NSG salinity approximately steady from year to year, is assessed to have an annual mean velocity of approximately 0.02m s^{-1}.

Some twelve large-scale surveys of salinity in NSG (and beyond) during the period July 1982 to January 1985 were used to evaluate spatial mean salinities of the whole NSG area (~500 km^2), and thus reveal the character of its seasonal and inter-annual variability. During the 30-month period, mean NSG salinity (or MNSGS) showed a variation from 40.90gl^{-1} to 42.57gl^{-1} with significant variation of the inter-annual range (rising by ~1.0gl^{-1} from late 1982 to early 1983, followed by a fall of ~1.8gl^{-1} through to late 1983). Two further surveys were conducted in mid-2008 and early 2009 and all data, spanning the entire 27-year period, were cross-calibrated using the same batch of standard seawater samples, which were themselves checked for accuracy using new standard samples.

Since evaporation is understood to be the primary cause of the salinity response in NSG, records of evaporation and precipitation from Meteorological Bureau stations were examined for their consistency and longevity, yielding useful daily data from Adelaide airport, Price and Spalding spanning the period 1982 to 2009. Assuming that the mean salinity of northern Spencer Gulf reflects, in a consistent measurable way, the integrated influences of net evaporation during a preceding period, comparison between the 1982-1985 mean NSG salinity and lagged-filtered net evaporation (at Price) showed that a lag of 192 days produced the optimum least squares fit. Thus, for the 30-month period involving twelve separate salinity surveys of NSG, the mean salinity was shown to closely reflect the cumulative effects of net evaporation for the 6-months prior to any particular observation. Comparison with Adelaide Airport and Spalding net evaporation data showed a similar result (achieving optimum results with a lag of 190 and 192 days respectively) although the fit to data showed slightly larger variances.

Using the optimum filter lag of 192 days on Price net evaporation, the analysis was extended through to 2009 showing that current NSG salinities remain approximately predictable using the 1980s calibration. Thus, even though the long-term record of lagged, filtered net evaporation showed strong inter-annual trends in the intervening years, it is apparent that NSG mean salinity on any particular day is primarily determined by the cumulative effects of net evaporation during the prior six months, and that the Gulf has essentially no 'memory' of longer term influences. This provides an answer to the first question about the way that northern Spencer Gulf responds to perturbations that influence salinity.

On the basis of this result, 192-day lagged, filtered, net evaporation (LMNE) from Price was used as a proxy indicator of mean NSG salinity (converted using the linear regression result: proxy salinity = (40.98 + 0.23*LMNE)gl^{-1}). This proxy measure implies that the mean salinity of NSG between 1982 and 2009 was 41.56gl^{-1}, the mean annual range was 1.38gl^{-1}, further modified by inter-annual trends in which the mean fell to 41.25gl^{-1} in 1997/98, and then rose to 42.02gl^{-1} in 2007/08. The proxy also indicated that the annual maximum salinity of NSG was, on average, reached on 12th April, and the annual minimum on 14th October, a span of almost exactly half a year, despite there being no *a priori* reason for the cycle to be symmetric since the assessment is interpreted from measurements of net evaporation.

Assuming that the effect of desalination may be considered equivalent to that of evaporation, the calibration obtained between mean NSG salinity and lagged, filtered evaporation was used to assess the expected impact of desalination on mean NSG salinity. The primary distinction between the two mechanisms relates to the zone in which freshwater is considered to be removed: for natural evaporation this is considered to be approximately uniform over the entire region whereas desalination is expected to withdraw fluid from a much more localised zone around the intake itself. In both cases the higher salinity northward flow that replaces fluid losses is assumed to occur more or less uniformly through the southern boundary. Thus, as far as the large-scale response of NSG is concerned, there should be no significant difference between desalination and environmental evaporation. It was also assumed that all of the desalination return water contribute to raising the salinity of NSG whereas, due to the proposed location of the outfalls, this is likely to overestimate the influence of desalination on NSG.

Given these assumptions, desalination yielding an average of 251 megalitres of freshwater per day is expected to raise the mean salinity of NSG by up to 0.11gl^{-1}, to a new mean of 41.67gl^{-1}. For comparison purposes, this shift of the mean represents 8% of the mean annual salinity variation in NSG, and approximately 15% of the variation of annual mean salinity inferred to have occurred between 1997/98 and 2007/08.

In the same way, the effects of climate change on NSG salinity were assessed using projections of precipitation in 2030 and 2070 reported by Suppiah et al (2006). The analysis used projected precipitation to estimate evaporation (based on regression between precipitation and evaporation at Adelaide airport between 1982 and 2009) yielding net evaporation. This process indicated increases of net evaporation in 2030 of 0.32 x 10^{-3} m day^{-1}, and in 2070 of 0.97 x 10^{-3} m day^{-1}. Using the calibration between NSG salinity and change of net evaporation indicates, based on predictions of precipitation changes, salinity increases in NSG of up to 0.07gl^{-1} (2030) and 0.22gl^{-1} (2070).

Projected changes of air and sea temperatures from Suppiah et al (2006) were also used to assess evaporation from bulk aerodynamic formulae, and combined with precipitation predictions to provide alternative estimates of net evaporation changes in 2030 and 2070. This approach indicated increases of net evaporation in 2030 of 0.21 x 10^{-3} m day^{-1}, and in 2070 of 0.71 x 10^{-3} m day^{-1}. These adjustments imply salinity increases in NSG of up to 0.05gl^{-1} (2030) and 0.16gl^{-1} (2070). This resolved the second of question about the extent of changes to the equilibrium salinity of northern Spencer Gulf associated with defined perturbations.

Finally, the origins of the oceanographic exchange mechanisms that discharge excess salt from the Gulf were examined in order to assess whether their contributions to equilibrium arrangements are, in any sense, precarious and potentially subject to irreversible disruption by perturbations associated with desalination or climate change (or their combination). The mechanisms that contribute to salt discharge are gravitational circulation and turbulent

diffusion and dispersion, both of which act to send excess salt southward from higher to lower salinities (i.e., down the salinity gradient).

Gravitational circulation creates spatially differentiated exchange flows (inflow and outflow, each occupying approximately half of any particular cross-section) which, in a non-rotating frame of reference would be vertically juxtaposed, separated by a horizontal interface and, in a rapidly rotating frame of reference, would be largely horizontally juxtaposed, separated by a vertical interface. The influence of the Earth's rotation in northern Spencer Gulf suggests an intermediate arrangement biased towards the rotating case, and thus the stability (or disruption) of the (tilted) interface can only affect a fraction of the exchange circulation, which is largely horizontally distinct. In this case, the only criterion that limits the magnitude of the exchange circulation away from the interface is that of the densimetric Froude number which does not, in any way, impose constraints on the circulation required to maintain the large-scale salt balance in the face of any foreseeable perturbation.

Similarly, the curvature of the salinity gradient is responsible for the dispersive discharge of salt, down the salinity gradient. Assuming that the gradient is logarithmic, implies that only a small adjustment is required to enhance the dispersive flux in response to a perturbation that raises NSG salinity. For example, a 10% increase of evaporation was assessed to require a change to the curvature of the salinity gradient that would raise the mean salinity by $0.18 gl^{-1}$. This mechanism is not limited in its ability to respond to any foreseeable perturbation to NSG salinity. Thus, as a response to the third question posed in this report, and without the need to define the precise mechanisms responsible for maintaining the long-term salt balance of NSG, it is nevertheless evident that the current equilibrium arrangement is expected to remain stable to disruption associated with the anticipated and predicted effects of desalination and climate change.

8 Acknowledgments

I would like to thank Dr John Bennett of Flinders University for his assistance in the use of the laboratory facilities and particularly the Auto-Lab bench salinometer used for analysing all salinity samples collected during the 2008 and 2009 surveys. I would also like to thank Professor Geoff Lennon, Dr David Bowers, Mr James Brook and Dr Daniel Botelho for helpful comments on the manuscript. The work was conducted while sub-contracted to ARUP Pty Ltd, and I thank Mr James Brook and Mr David Wiltshire for their support and encouragement in this endeavour.

9 References

BHP Billiton, 2009, *Olympic Dam Expansion: Draft Environmental Impact Statement 2009*.

Brutsaert, W., 1982, *Evaporation Into The Atmosphere: Theory, History and Applications*, Reidel Publishing Company, ISBN 90-277-1247-6.

Bye, J.A.T., 1981, Exchange processes for Upper Spencer Gulf, South Australia, *Transactions of the Royal Society of South Australia*, 105(2), 59-66.

Farquhar, G.D. & M.L. Roderick, 2005, The pan evaporation paradox – an overview of the scope of the problem, *Proceedings of a workshop held at the Australian Academy of Sciences*, 22-23 Nov 2004

Fischer, H.B., E.J. List, R.C.Y. Koh, J. Imberger & N.H. Brooks, 1979, *Mixing in Inland and Coastal Waters*, Academic Press, ISBN 0-12-258150-4.

Gifford, R, 2005, Pan evaporation: an example of the detection and attribution of trends in climate variables, *Proceedings of a workshop held at the Australian Academy of Sciences*, 22-23 Nov 2004.

Holloway, P.E., 1980, A criterion for thermal stratification in a wind-mixed system, *Journal of Physical Oceanography*, 10(6), 861-869.

Hounam, C.E., 1973, *Comparison Between Pan and Lake Evaporation*, World Meteorological Organization Technical Note 126, 52pp, Geneva.

Johnson, F. & A. Sharma, 2007, Estimating Evaporation – Issues and Challenges, in: D. Kulasiri and L. Oxley (Editors), *MODSIM 2007 Congress,* Modelling and Simulation Society of Australia and New Zealand, Christchurch, New Zealand

Lennon, G.W., D. Bowers, R.A. Nunes, B.D. Scott, M. Ali, J. Boyle, C. Wenju, M. Herzfeld, G. Johansson, S. Nield, P. Petrusevics, P. Stephenson, A. Suskin & S.E.A. Wijffels, 1987, Gravity currents and the release of salt from an inverse estuary, *Nature*, 327, 695-697.

Linacre, E.T. 1994. Estimating U.S. Class A pan evaporation from few climate data. *Water International*, 19, 5-14.

Linacre, E.T., 2005, Lake E_o, pan E_p, actual (terrestrial) E_a, potential E_t and ocean evaporation rates, *Proceedings of a workshop held at the Australian Academy of Sciences*, 22-23 Nov 2004.

Nunes, R.A., 1985, Catalogue of data from a systematic programme of oceanographic measurements in Spencer Gulf from 1982 to 1985, *Cruise Report 10*, Flinders Institute for Atmospheric & Marine Science, Flinders University of South Australia.

Nunes, R.A. & G.W. Lennon, 1986, Physical property distributions and seasonal trends in Spencer Gulf, South Australia: an inverse estuary, *Australian Journal of Marine & Freshwater Research*, 37(1), 39-53.

Nunes, R.A. & G.W. Lennon, 1987, Episodic Stratification and Gravity Currents in a Marine Environment of Modulated Turbulence, Journal of Geophysical Research, 92(C5), 5465-5480.

Nunes Vaz, R.A., G.W. Lennon and D.G. Bowers, 1990, Physical behaviour of a large, negative or inverse estuary, *Continental Shelf Research*, 10(3), 277-304.

Ou, H.W., 1984, Geostrophic adjustment: a mechanism for frontogenesis, *Journal of Physical Oceanography*, 14, 994-1000.

Petrusevics, P.M., 1993, SST Fronts in Inverse Estuaries, South Australia – indicators of reduced gulf-shelf exchange, *Australian Journal of Marine & Freshwater Research* 44(2), 305-323.

Roderick, M., M. Hobbins & G. Farquhar, 2009, Pan Evaporation Trends and the Terrestrial Water Balance. I. Principles and Observations, *Geography Compass*, 3(2), 746-760.

Suppiah, R., B. Preston, P.H. Whetton, K.L. McInnes, R.N. Jones, I. Macadam, J. Bathols & D. Kirono, 2006, *Climate change under enhanced greenhouse conditions in South Australia: an updated report on assessment of climate change, impacts and risk management strategies relevant to South Australia*, Commonwealth Scientific & Industrial Research Organisation, Division of Marine and Atmospheric Research, http://www.climatechange.sa.gov.au/uploads/pdf/SA_CMAR_Exec_Summary.pdf

Turner, J.S., 1973, *Buoyancy Effects in Fluids*, Cambridge University Press, 368pp.

Whitehead, J.A., 1998, Multiple T-S States for Estuaries, Shelves, and Marginal Seas, *Estuaries* 21(2), 281-293.

Appendix A

New Salinity Surveys of Northern Spencer Gulf

In the course of this study new salinity data were collected from northern Spencer Gulf. This Appendix formally records the data and results: all data from 1980s surveys were reported in Nunes (1985).

Water samples from the bottom were collected using a Nansen bottle by lowering to the sea bed, and then raising the bottle approximately half a metre before triggering its mechanism to capture the sample. Surface samples were collected using a bucket that was well rinsed at each new station. Where the total depth was less than approximately two metres, only one water sample was collected.

Each water sample was decanted into two collection bottles to provide a check when these were analysed back in the laboratory. The method of analysis was described in the main text of this report. Most bottle pairs differed, in the analysis, by no more than 0.02 but discrepancies were found for bottle 39 on 6th August 2008 (where the reading from the salinometer was clearly in error).

Survey of 6th August 2008

Salinity Survey of Upper Spencer Gulf 6th August 2008						
Station	**Latitude**	**Longitude**	**Time**	**Bottle**	**Depth**	**Salinity**
1	32 59.88	137 47.63	0818	1	16m	41.24
				2		41.22
				3	Surface	41.25
				4		41.23
2	32 59.79	137 49.40	0830	5	23m	41.18
				6		41.17
				7	Surface	41.19
				8		41.20
3	32 59.85	137 52.74	0855	9	12m	41.42
				10		41.41
				11	Surface	41.36
				12		41.38
4	32 59.86	137 55.83	0910	13	7m	41.61
				14		41.59
5	32 56.59	137 46.47	1005	15	Surface	41.45
				16		41.44
				17	18m	41.43
				18		41.44
6	32 54.64	137 47.35	1025	19	Surface	41.40
				20		41.40
				21	18m	41.48
				22		41.49
7	32 54.53	137 50.31	1041	23	Surface	41.77
				24		41.77
				25	18m	41.81
				26		41.81
8	32 54.53	137 54.49	1108	27	Surface	42.13
				28		42.12

9	32 50.01	137 52.99	1120	29	Surface	42.04
				30		42.06
10	32 50.01	137 50.70	1150	31	Surface	42.02
				32		42.03
				33	12m	42.00
				34		42.00
11	32 50.01	137 49.32	1206	35	Surface	41.88
				36		41.87
				37	4m	41.85
				38		41.86
12	32 45.01	137 49.70	1235	39	Surface	error
				40		42.71
				41	12m	42.66
				42		42.66
13	32 45.00	137 53.19	1255	43	Surface	42.83
				44		42.83
14	32 42.13	137 47.13	1319	45	Surface	43.09
				46		43.11
15	32 41.88	137 47.32	1327	47	13m	43.11
				48		43.12
				49	Surface	42.97
				50		42.97
16	32 41.40	137 48.12	1345	51	Surface	43.18
				52		43.19
17	32 37.50	137 46.50	1400	53	Surface	43.32
				54		43.33
18	32 34.03	137 45.86	1425	55	Surface	44.15
				56		44.15
				57	6m	44.23
				58		44.24
19	32 32.48	137 46.80	1440	59	Surface	44.49
				60		44.49
				61	11m	44.55
				62		44.55

As the data indicate, most stations were reasonably well mixed in the vertical. Depth-averaged salinities were determined for each station (by averaging surface and bottom salinities), plotted and contoured in Fig A.1

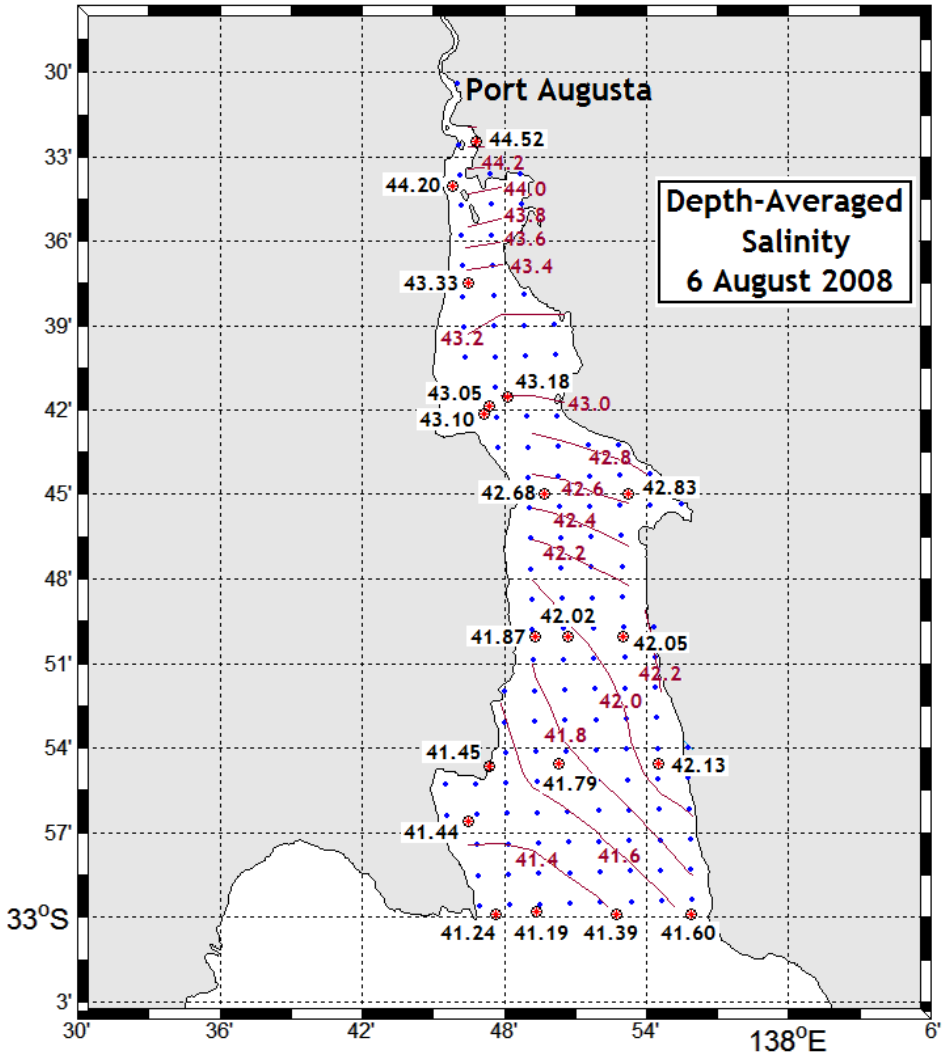

Figure A1. Salinity samples were collected from locations indicated with red-filled circles. These were interpolated onto the regular 2km x 2km grid shown as blue dots, and contoured as shown. These results represent the salinity of northern Spencer Gulf as sampled on 6th August 2008.

Survey of 2nd March 2009

Salinity Survey of Upper Spencer Gulf 2nd March 2009						
Station	**Latitude**	**Longitude**	**Time**	**Bottle**	**Depth**	**Salinity**
1	33 0.13	137 47.54	0845	1	27m	41.73
				2		41.74
				3	Surface	41.22
				4		41.21
2	33 0.10	137 49.58	0905	5	23m	42.04
				6		42.04
				7	Surface	41.96
				8		41.97
3	33 0.09	137 52.72	0920	9	10m	42.12
				10		42.12

				11	Surface	42.13
				12		42.13
4	33 0.09	137 55.80	0935	13	6m	42.27
				14		42.26
				15	Surface	42.26
				16		42.26
5	32 58.88	137 52.88	0950	17	12m	42.12
				18		42.12
				19	Surface	42.14
				20		42.14
6	32 56.59	137 46.48	1015	21	18m	42.15
				22		42.14
				23	Surface	42.04
				24		42.04
7	32 54.71	137 47.56	1027	25	8m	42.23
				26		42.23
				27	Surface	42.26
				28		42.26
8	32 54.53	137 50.32	1040	29	21m	42.65
				30		42.64
				31	Surface	42.56
				32		42.57
9	32 54.53	137 54.49	1057	33	Surface	42.45
				34		42.46
10	32 50.01	137 52.99	1115	35	2.5m	42.53
				36		42.53
11	32 50.01	137 50.70	1125	37	12m	42.84
				38		42.84
				39	Surface	42.81
				40		42.81
12	32 50.00	13749.31	1135	41	12m	42.8
				42		42.79
				43	Surface	42.55
				44		42.55
13	32 45.01	137 49.70	1155	45	12m	43.38
				46		43.37
				47	Surface	43.27
				48		43.27
14	32 45.01	137 53.19	1210	49	2.5m	43.55
				50		43.55
15	32 41.88	137 47.32	1235	51	12m	44.10
				52		44.10
				53	Surface	43.99
				54		44.00
16	32 41.49	137 47.99	1240	55	3m	44.16
				56		44.14
17	32 37.51	137 46.43	1300	57	11m	44.96
				58		44.96
				59	Surface	44.72
				60		44.72
18	32 34.04	137 45.86	1315	61	8m	45.45
				62		45.45

				63	Surface	45.43
				64		45.44
19	32 32.48	137 46.79	1325	65	Surface	46.47
				66		46.48
				67	11m	46.03
				68		46.04

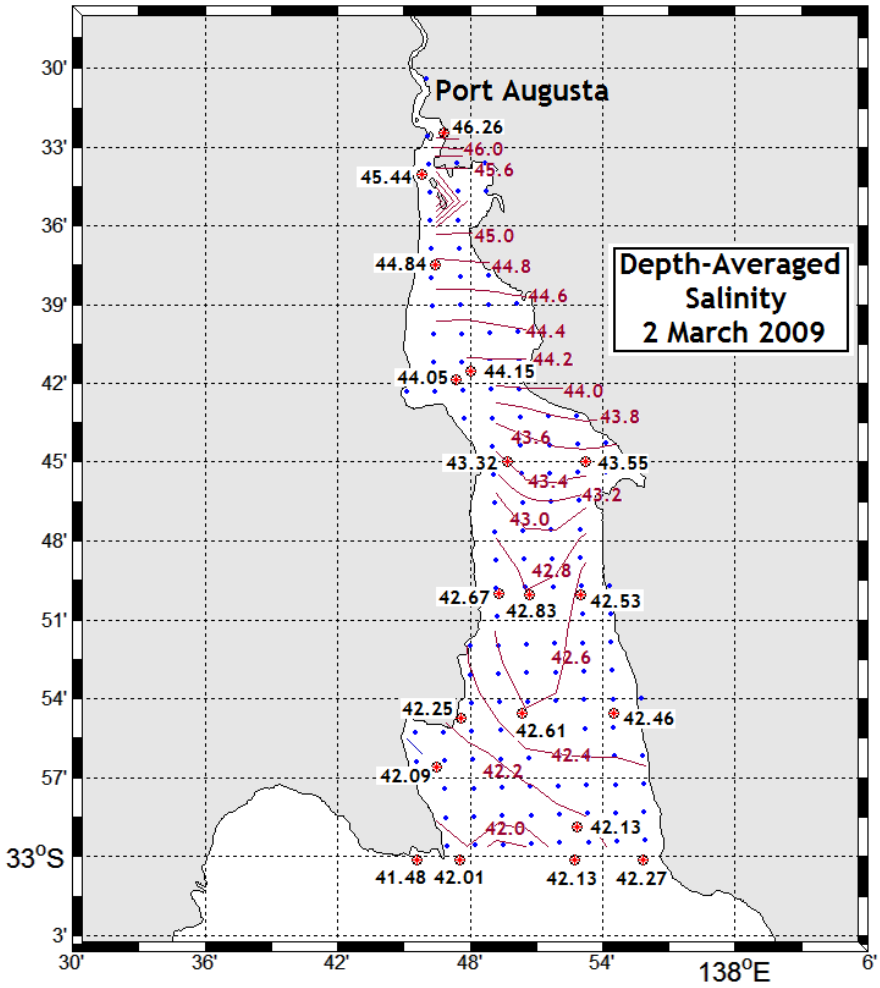

Figure A2. Salinity samples were collected from locations indicated with red-filled circles. These were interpolated onto the regular 2km x 2km grid shown as blue dots, and contoured as shown. These results represent the salinity of northern Spencer Gulf as sampled on 2nd March 2009.

APPENDIX H8.2

Water exchange rate calculations

H8.2 WATER EXCHANGE RATE CALCULATIONS

Table H8.2.1 provides the details of calculations used to support a response in Section 17.6.1 of the Supplementary EIS.

Table H8.2.1: Calculations of water exchange across a boundary at Point Lowly

Step	Parameter	Source	Draft EIS	Supplementary EIS
1	Annual evaporation in NSG[1]	As per notes	2 m[2]	1.38 m[3]
2	Mean depth of NSG	As per notes	9 m[4]	8.4 m[5]
3	Percentage of NSG waters evaporated	Calculated from step [1] / [2]	22%	16.5%
4	Mean salinity of NSG	As per notes	43.5[6]	42.7[7]
5	Salinity at Point Lowly	As per notes	41[6]	42.1[7]
6	Salinity increase from Point Lowly water replacing evaporated water (without exchange)	Calculated from [3] * [5] + [4]	52.6	49.6
7	Percentage of water required to exchange across Point Lowly boundary (F) to restore previous salinity	F * [5] + (1-F) * [6] = [4], hence F = [3] * [5] / ([4] - [5] + [3] * [5])	78%	92%

Notes:
1 Northern Spencer Gulf.
2 Rounded estimate from meteorological data.
3 See Appendix H8.1 of the Supplementary EIS.
4 Rounded estimate from GIS data.
5 See Appendix H8.1 of the Supplementary EIS.
6 Based on average annual salinities at Point Lowly and Port Augusta of 41 g/L and 46 g/L respectively (Nunes and Lennon 1986). The midpoint of this range was used as a conservative average salinity in NSG (refer Section 16.6.4 of the Draft EIS).
7 Based on data collected in March 2009 (see Appendix H8.1 of the Supplementary EIS). Salinity at Point Lowly is the mean of measurements eastward from Point Lowly. Note that data collected in August 2008 (mean salinity 42.0 g/L, southern boundary mean 41.4 g/L) would result in the same exchange rate as for March 2009.